General Disclaimer

One or more of the Following Statements may affect this Document

- This document has been reproduced from the best copy furnished by the organizational source. It is being released in the interest of making available as much information as possible.

- This document may contain data, which exceeds the sheet parameters. It was furnished in this condition by the organizational source and is the best copy available.

- This document may contain tone-on-tone or color graphs, charts and/or pictures, which have been reproduced in black and white.

- This document is paginated as submitted by the original source.

- Portions of this document are not fully legible due to the historical nature of some of the material. However, it is the best reproduction available from the original submission.

Produced by the NASA Center for Aerospace Information (CASI)

AN ADVANCED 10.6-MICRON LASER COMMUNICATION EXPERIMENT

JOHN H. McELROY
NELSON McAVOY
HERBERT L. RICHARD
WILLIAM E. RICHARDS
STEVEN C. FLAGIELLO

NOVEMBER 1968

GSFC ——— GODDARD SPACE FLIGHT CENTER ———
GREENBELT, MARYLAND

AN ADVANCED 10.6-MICRON LASER

COMMUNICATION EXPERIMENT

John H. McElroy
Nelson McAvoy
Herbert L. Richard
William E. Richards
Steven C. Flagiello

Advanced Development Division

November 1968

GODDARD SPACE FLIGHT CENTER
Greenbelt, Maryland

AN ADVANCED 10.6-MICRON LASER

COMMUNICATION EXPERIMENT

John H. McElroy
Nelson McAvoy
Herbert L. Richard
William E. Richards
Steven C. Flagiello
Advanced Development Division

ABSTRACT

The purpose of the laser intersatellite communication experiment proposed in this document is to determine the capability of the carbon dioxide laser to meet the high data-rate, intersatellite communication requirements envisioned for the late 1970's and 1980's. The experimental package to be developed consists of two systems: a 100 MHz bandwidth communication unit for synchronous satellite to synchronous satellite applications and a 5 MHz bandwidth communication unit for low-altitude satellite to synchronous satellite applications.

The proposed development will result in the production of a complete breadboard communication system, in near space-qualified form, that will be available in 1972 for use in appropriate spacecraft during the 1970's. The system will be developed to the point that placing the experimental package on a given satellite will consist primarily of space-qualification, packaging, interfacing the system to the spacecraft, and test and evaluation.

TABLE OF CONTENTS

TABLE OF CONTENTS (Continued)

ILLUSTRATIONS

ILLUSTRATIONS (Continued)

ACKNOWLEDGMENT

AN ADVANCED 10.6-MICRON LASER

COMMUNICATION EXPERIMENT

1. INTRODUCTION

It is proposed that development be started on an advanced 10.6-micron laser communication experiment. The purpose of the experiment is to study high data-rate communication between satellites. The experimental package to be developed consists of two systems. The first system will provide a 100 MHz information bandwidth channel between two synchronous satellites. The second system will provide a 5 MHz information bandwidth channel between a satellite in a low-altitude Earth orbit and a second satellite in synchronous orbit.

The proliferation of Earth-orbiting satellites and the attendant collection of data gathered by these satellites, have created difficult mission support requirements. The employment of ground stations, ships, and aircraft to receive the collected data has severe limitations. Even the more than one hundred communication terminals currently used for satellite communications cannot give adequate coverage to all desired missions; a given ground station can view only a small portion of a single orbit and only a fraction of the total number of orbits of a satellite. This is particularly true for low-altitude satellites, such as the planned Earth Resources Technology Satellites (ERTS). Complete coverage of such orbits would require many more stations than currently exist or could be supported economically.

Two approaches can be used to circumvent this problem. First, if on-board, high-capacity storage could be incorporated in the low-altitude satellites, the collected information could be stored until the satellite came in view of a ground station, at which time the stored information could be "dumped" via a high data rate channel. For some planned missions, higher storage capacities would be required than can be predicted to be feasible in the near future. In addition, the high data rate "dump" channel may require a prohibitively wide bandwidth for a small satellite.

The second approach to the problem is the Data Relay Satellite System. A group of three satellites equally spaced in synchronous orbit could serve as data collection centers for the information gathered by low-altitude satellites. Very wideband relay channels could then carry the data to a synchronous satellite in view of the continental United States which would beam the information to a ground terminal.

The implementation of the Data Relay Satellite concept necessitates the establishment of wide bandwidth inter-satellite communication links. When conventional microwave or millimeter wave systems are examined, it is found that the prime power and weight requirements for such a link are, at best, exorbitant. Recent advances in laser technology have shown that a laser system can be a serious contender for application in inter-satellite communication links. In this application the laser has become an attractive alternative to microwaves and millimeter waves. Further, the use of laser frequencies gives relief to the already crowded frequency spectrum in the region up to 10 GHz.

The objectives of the proposed Advanced 10.6-Micron Laser Communication Experiment (ALCE) are:

1. To measure the communication performance of a spaceborne inter-satellite laser communication system (data quality, signal-to-noise ratios as functions of various parameters, etc.)

2. To measure the tracking and acquisition servo loop parameters of optical autotrack systems in the space environment.

3. To measure the performance of laser communication system components in space.

The salient characteristics of the system proposed for development under the Earth Oriented Applications in the Advanced Applications Flight Experiments Program are:

100-MHz Synchronous Satellite to Synchronous Satellite Link

(Duplicate systems are assumed to be on-board each satellite)

Information Bandwidth:	100 MHz
Prime Power Requirements:	200 watts
Mass:	34 kg
Optical Antenna Diameter (Receiver and transmitter):	25 cm
Antenna Gain:	98.5 db
Receiver Sensitivity:	-160 dbm/Hz
Intermediate Frequency:	150 MHz
Effective Radiated Power (ERP):	1.2 watts

Transmitter Efficiency:	10%
Transmitter Transmission Losses:	3 db
Laser Transmitter Power Output:	2.4 watts
Signal-to-Noise Power Ratio from Optical Mixer:	30 db
Receiver Transmission Losses:	10 db
Range: (Between two satellites in tri-satellite DRS system)	7.35×10^7 m

Low-Altitude to Synchronous Satellite Link

5 MHz Up-Link

(Receiver parameters refer to the receiver on-board the synchronous satellite and transmitter parameters are those for the laser transmitter on-board the low altitude satellite)

Information Bandwidth:		5 MHz
Prime Power Requirements:		75 watts
Mass: (Complete Low-altitude satellite communication system)		20 kg
Optical Antenna Diameter:	Receiver:	25 cm
	Transmitter:	12.5 cm
Antenna Gain:	Receiver:	98.5 db
	Transmitter:	92.4 db
Receiver Sensitivity:		-160 dbm/Hz
Intermediate Frequency:		10 MHz - 1.35 GHz
Effective Radiated Power (ERP):		1.1 watts
Transmitter Efficiency:		10%
Transmitter Transmission Losses:		3 db
Laser Transmitter Power Output:		2.2 watts
Signal-to-Noise Power Ratio from Optical Mixer:		30 db
Receiver Transmission Losses:		10 db
Range: (For illustration, the maximum range from an ATS satellite to a Nimbus satellite was assumed)		5×10^7 m

Beacon Down-Link

(Receiver parameters refer to the receiver on-board the low-altitude satellite and transmitter parameters are those for the beacon transmitter and optical system on-board the synchronous satellite)

Information Bandwidth:		1 MHz
Prime Power Requirements:		20 watts
Weight:		10 kg
Optical Antenna Diameter	Receiver:	12.5 cm
	Transmitter:	25 cm
Antenna Gain:	Receiver:	92.4 db
	Transmitter:	98.5 db
Receiver Sensitivity:		-160 dbm/Hz
Intermediate Frequency:		10 MHz - 1.35 GHz
Effective Radiated Power (ERP):		0.22 watt
Transmitter Efficiency:		10%
Transmitter Transmission Losses:		3 db
Laser Beacon Transmitter Power Output:		0.44 watt
Signal-to-Noise Power Ratio from Optical Mixer:		30 db (after acquisition)
Beacon Tone Modulation Frequency (Produced by piezoelectric modulation of laser frequency):		1 MHz
Receiver Transmission Losses:		10 db
Range:		5×10^7 m

The result of this program will be the production of a breadboard model of the system in near space-qualified form. The development will proceed in parallel on a subsystem basis. The pertinent subsystems are the transmitter/modulator subsystem, receiver subsystem, and tracking and acquisition subsystem.
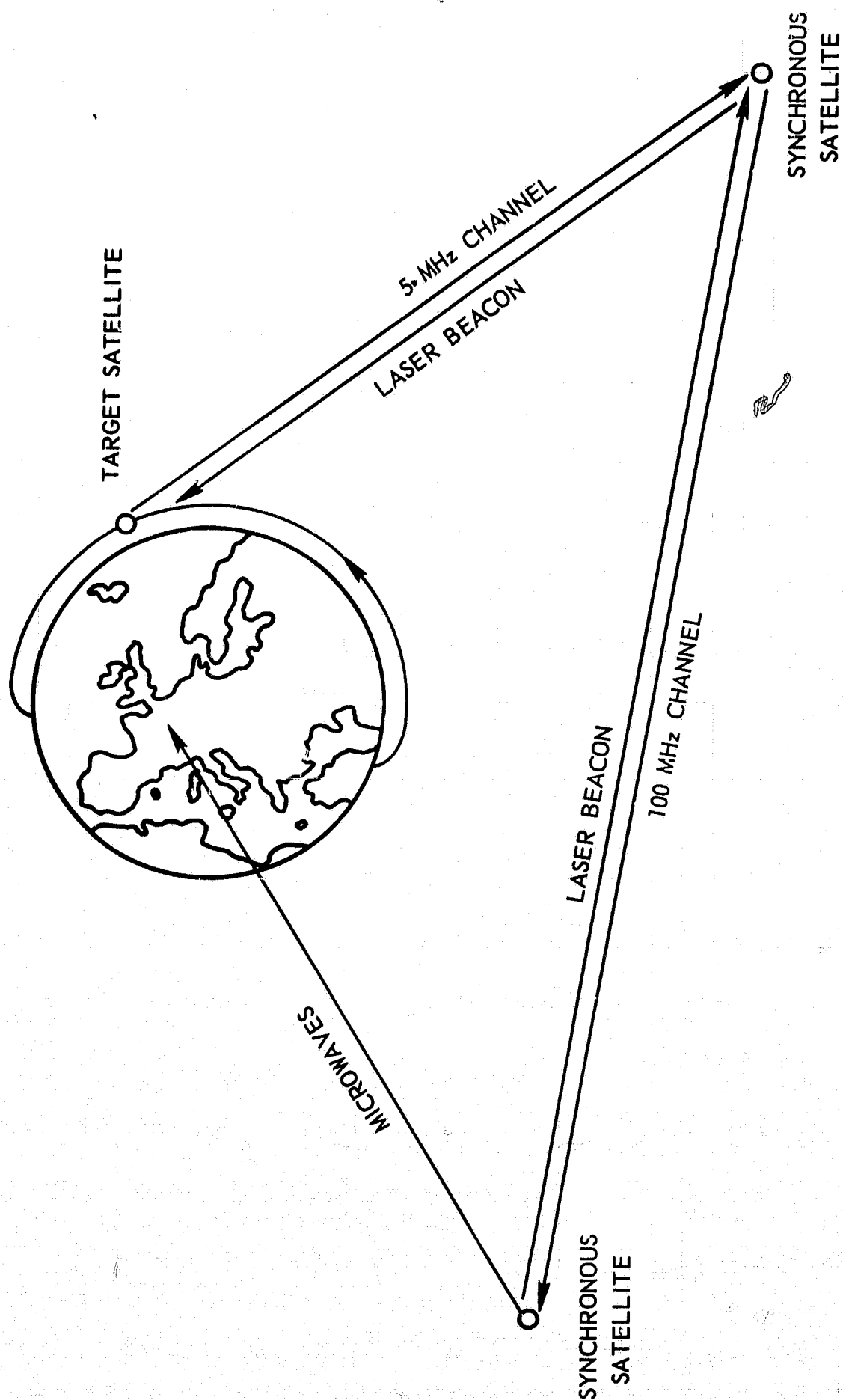
Figure 1-1. Advanced 10.6-micron laser communication experiment

SYNCHRONOUS SATELLITE

TARGET SATELLITE

5-MHz CHANNEL

LASER BEACON

100 MHz CHANNEL

LASER BEACON

MICROWAVES

SYNCHRONOUS SATELLITE

2. INSTRUMENTATION

The instrumentation for the ALCE represents an extension of the equipment currently being designed for the ATS-F satellite and the equipment for the proposed ATS-F to ATS-G intersatellite communication link.[1] It differs in the following respects: Information bandwidth, 100 MHz versus 5 MHz; optical antenna diameter (25 cm versus 12.7 cm), which requires improved pointing and tracking; and the ability of the advanced system to accommodate the high Doppler shifts (up to 1.35 GHz) that will be present in the channel between the synchronous satellite and the low-altitude satellite. Each of the differences is a highly significant advance.

The carbon dioxide laser is an attractive transmitter in a space-to-space communication system for a number of reasons. Perhaps, the most fundamental of the reasons is its ability to produce high output powers with high efficiency. Multikilowatt continuous powers at efficiencies in excess of 25% have been reported. In the laboratories of the Optical Systems Branch, multimode power outputs in excess of six watts have been obtained routinely from carbon dioxide lasers with an active discharge length of only 30 cm. When these lasers are restricted to single-mode operation, as is necessary for communications work, more than 2 watts are available. This is the approximate power output required for the ALCE.

In addition to the features of high power and high efficiency, the wavelength of the output radiation from a CO_2 laser is favorable from a number of viewpoints. As is well known, the gain of an antenna increases with increasing frequency (neglecting fabrication difficulties temporarily). The gain of any antenna will, in general, be equal to or less than

$$ G = \frac{4\pi D^2}{\lambda^2} \tag{2-1} $$

where D is the diameter of the antenna and λ is the wavelength of the transmitted radiation. It has been assumed that the solid angle of the emitted radiation is given by $(\lambda/D)^2$ and is defined by the half-power points on the radiation pattern. Therefore, from the standpoint of Equation (2-1), a communication system should operate at the highest frequency possible. When coupled with the wide bandwidths that can be utilized and the empty frequency spectrum at laser frequencies, the potential of the laser in intersatellite communications is clear.

In order to make a practical judgement, however, it must also be acknowledged that fabrication of components and maintenance of the alignment of components becomes more difficult at higher frequencies. From this qualitative argument it is clear that an optimum communication frequency (from the standpoint of the antenna) is at the highest frequency permitted by mechanical fabrication and alignment tolerances. Dimeff, et al., have derived an empirical expression for the wavelength dependence of the attainable spaceborne antenna radius.[2] If this equation is inserted into Equation (2-1), the resulting wavelength dependence of attainable antenna gain is given by

$$G = \frac{4\pi(8.06 \times 10^2 \times \lambda^{0.48})}{\lambda^2} = 1.95 \times 10^{-9} \, f^{1.52} \qquad (2\text{-}2)$$

where f is the transmitted carrier frequency. A plot of this equation is shown in Figure 2-1. The dashed curve at the upper right of the graph represents a plausible correction that would convert the curve from showing what it is believed can be developed in the middle 1970's, a somewhat speculative effort, to what should be attainable today with relatively little developmental work. From this curve it can be seen that antenna gains at 10.6 microns are 60 db higher than present microwave antennas.

Using Equation (2-2) it is simple to derive, from the range equation, the power collected by the receiver aperture. The derivation of this equation is given in Appendix A. The result is

$$P_R = 6.5 \times 10^5 \, P_T \, \lambda^{-1.04}/R^2 \qquad (2\text{-}3)$$

where P_T is the effective radiated power and R is the range. The noise power per cycle of bandwidth is given by

$$P_N/B = \frac{hf}{e^{hf/kT} - 1} + hf \qquad (2\text{-}4)$$

where k is Boltzmann's constant and T is the noise temperature in degrees Kelvin. Therefore, the signal-to-noise power ratio is given by
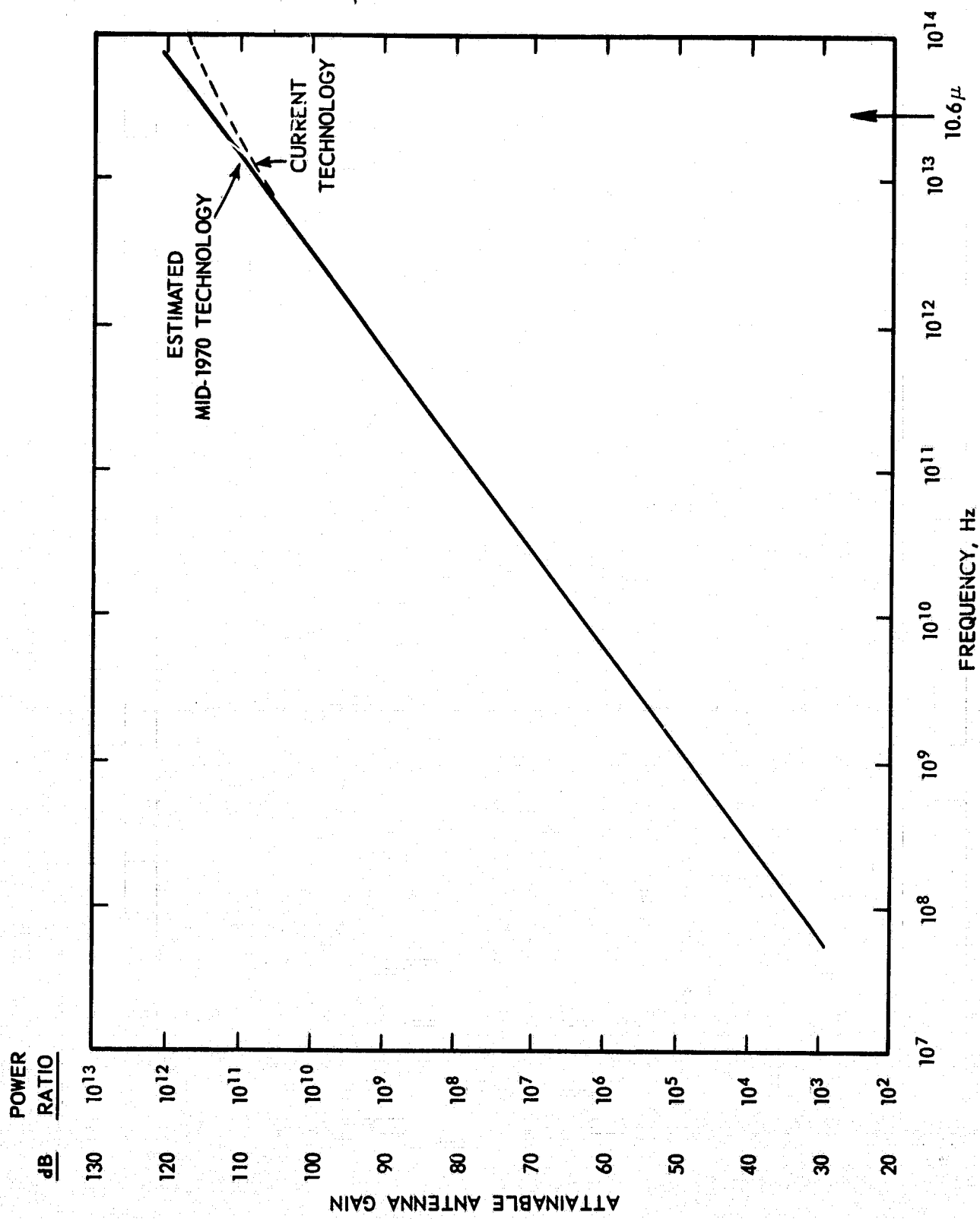
Figure 2-1. Attainable antenna gain versus frequency.

$$(S/N)_P = P_S/P_N = \frac{P_T\,T_R \times 6.5 \times 10^5\,\lambda^{-1.04}}{R^2\left(\dfrac{hf}{e^{hf/kT}-1} + hf\right)B} \qquad (2\text{-}5)$$

where B is the receiver noise bandwidth and T_R is the transmittance of the optical system between the receiver aperture and the signal detector. From the preceding equations it is now possible to write an equation giving the wavelength dependence of the required effective radiated power, for constant signal-to-noise and range:

$$P_T = \frac{R^2\,(S/N)_P\,P_N\,\lambda^{1.04}}{6.5 \times 10^5\,T_R} = K\,P_N(\lambda)\,\lambda^{1.04} \qquad (2\text{-}6)$$

where K is merely a defined normalization factor used to remove all but wavelength dependent terms. The normalized power per unit bandwidth is plotted in Figure 2-2. It can be seen that the curve dips to a minimum in the vicinity of 10.6 microns. The minimum occurs at 48 microns. Once again the dashed curve has the same meaning as in Figure 2-1, namely, that of showing the capability of present technology. It shows that current technology sharpens the dip near 10.6 microns and, therefore, accentuates the conclusion that for a given signal-to-noise ratio the carbon dioxide laser communication system can carry more information for a given effective radiated power in an intersatellite communication system. From an experimental viewpoint, this conclusion is reinforced by the existence of an atmospheric window at 10.6 microns, which permits testing and experimentation between a satellite and a ground station.

A brief description will now be given of the envisioned experimental packages. The synchronous satellite to synchronous satellite communication package will be discussed first, followed by package on the synchronous satellite that will communicate with the low-altitude satellite, and, finally, the package on the low-altitude satellite that will communicate with the synchronous satellite.

2.1 SYNCHRONOUS SATELLITE TO SYNCHRONOUS SATELLITE COMMUNICATION SYSTEM

A conceptual drawing of the synchronous satellite to synchronous satellite communication package is shown in Figure 2-3. The experimental package on each satellite consists of five parts:

Figure 2-2. Normalized effective required radiated power per cycle of bandwidth versus frequency

- The optical subsystem containing a coarse beam-pointing mechanism (slewing mirror), a 25 cm Cassegrainian telescope, image-motion compensator, directive mirrors, and beam splitters.

- The laser subsystem containing the 2.4-watt laser transmitter and 100-MHz bandwidth modulator, the 100-mw laser local oscillator, the frequency stabilization servomechanism, and the laser power meters.

- The detector subsystem containing the signal information detector, detector preamplifiers, image-motion detector, and radiation cooler.

- The signal-processing subsystem containing the intermediate-frequency (IF) amplifiers, image-motion compensator drive electronics, laser transmitter modulator drive electronics, laser frequency-control

COARSE POINTING MECHANISM

CASSEGRAINIAN TELESCOPE

IMAGE-MOTION COMPENSATOR

POWER METERS

LASER L.O.

LASER XMTR/MODULATOR

VIEWING PORT

BEAM DIAMETER

DETECTORS

RADIATION COOLER

Figure 2-3. Laser system conceptual drawing, synchronous to synchronous satellite system

electronics, beam-pointing mechanism drive electronics, and command and telemetry interface electronics.

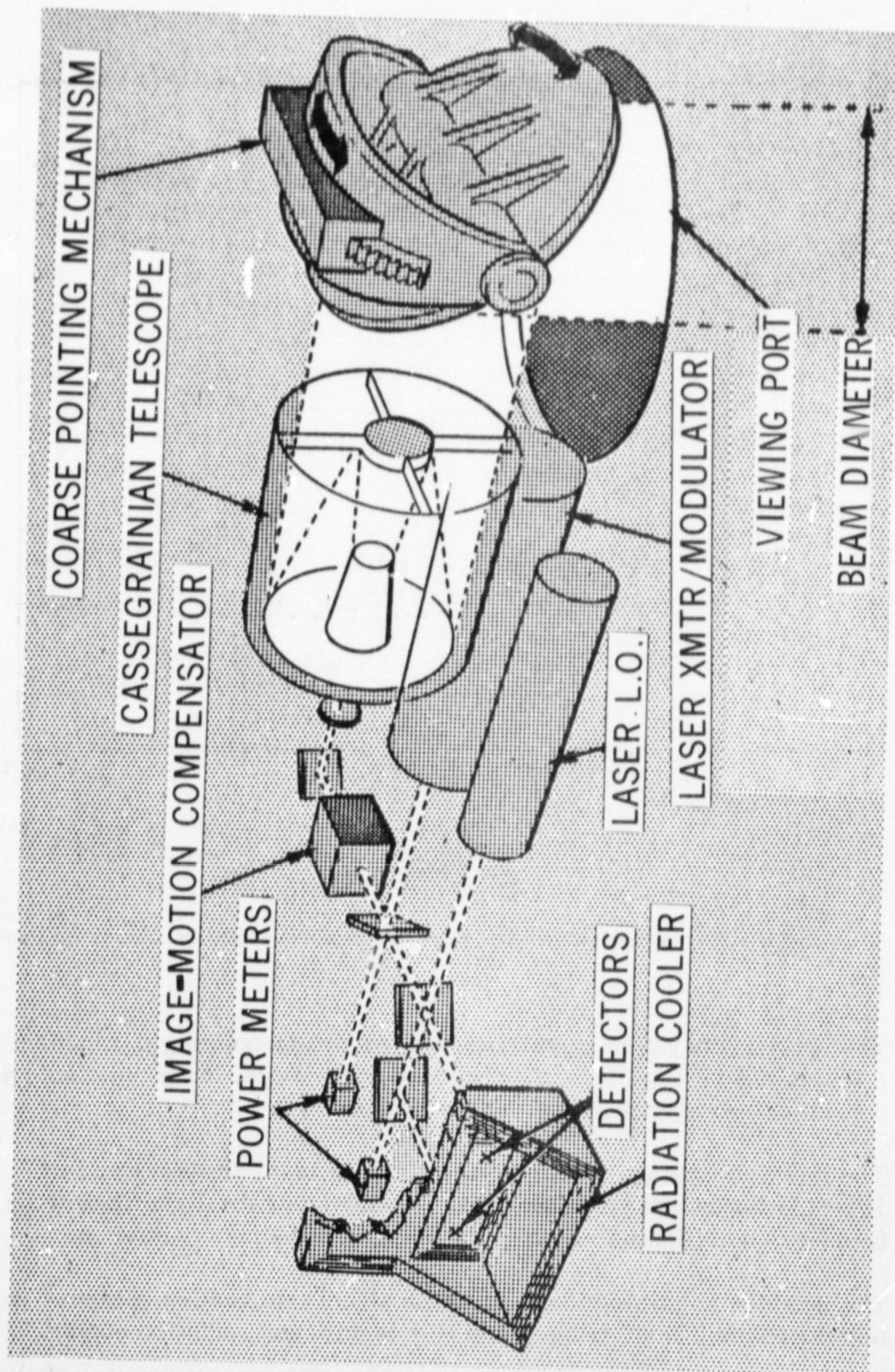- The power supply subsystem containing the laser high-voltage and modulator power supplies and the low-voltage signal processing and drive electronics power supplies.

2.1.1 OPTICAL SUBSYSTEM

The optical subsystem is designed to scan the transmitted beam and receiver over the acquisition field-of-view, form a narrow transmitted beam, collect energy in the infrared portion of the spectrum, divide it between image-motion sensor and information detector, and superimpose local oscillator and received radiation to produce heterodyne action.

2.1.1.1 COARSE BEAM-POINTING MECHANISM

The coarse beam-pointing mechanism serves to direct the transmitted beam and to channel the received laser signal into the Cassegrainian telescope. It is assumed that a single synchronous satellite will be the first element in the laser communication system to be orbited. During the period between the launch of the first satellite and the orbiting of the second, testing of the performance of the experimental package and experimentation will be conducted between the satellite and a ground station. The coarse beam-pointing mechanism will, therefore, be designed with the capability to steer the beam to any point on the Earth within an area approximately the size of the United States, as well as to the planned second synchronous satellite. If we assume a synchronous satellite over the Equator communicating with a second synchronous satellite positioned for a tri-satellite DRS system, including a generous margin for error in the position of the second satellite, this requires displacing the laser beam ±40 degrees from local nadir. In the north-south direction a displacement of ±5 degrees gives ample coverage of the Earth's surface.

The bearing on the 25-cm coarse pointing mirror will not experience much motion during the satellite lifetime. Except during the acquisition phase, corrections to the beam direction will be accomplished by a fine-control mechanism; therefore, very little repetitive positional movement is required of the coarse beam-pointing mechanism. Nevertheless, care will be exercised to provide the proper bearing lubrication for the mirror movement. For instance, vapor lubrication using a labyrinth bearing seal has operated for extended periods in space environments. This item is the only mechanically rotating mechanism in the system.

The coarse-pointing mechanism is a lightweight mirror consisting of aluminum or beryllium overcoated with 0.006 ± 0.001 inch of Kanegen before optical polishing. Metal mirrors are especially attractive because of their light weight, ease of mounting, high modulus of elasticity, and favorable thermal properties. For the 10.6-micron wavelength, the mirror flatness is not seriously degraded in the expected space environment and can be achieved more easily than in the visible wavelengths.

The viewing field of the optical subsystem is governed by several factors: the placement of the satellites, the location of the package on the satellite, and obscuration by the satellite structure. In all cases below, it will be assumed that these factors have been taken into consideration and that a suitable compromise has been reached.

2.1.1.2 OPTICAL ANTENNA

The optical antenna is a 25-cm diameter Cassegrainian, or off-axis telescope with a 0.1-degree field-of-view. It performs the same function as an RF antenna; it focuses the laser output into a high power-density beam during transmission and provides maximum power-gathering area during reception.

The mirrors are made from aluminum or beryllium overcoated with Kanegen. After optical polishing, the mirrors are coated with vacuum-deposited aluminum, either pure or in combination with other materials, to provide high-infrared but low-visible reflectance, see Figure 2-4. These films, as well as pure aluminum, provide a reflectance as high as 98 percent at 10.6 microns.[3] Special paints and baffles used in the telescope and telescope housing will reduce scattered light and provide temperature control. Because many of the optical elements and associated mounting structures radiate thermally to deep space, the mirrors themselves will operate at a temperature somewhat lower than that of the surrounding satellite. This can be advantageous because cold optical elements emit less background blackbody radiation; furthermore, it may be desirable to decouple them thermally from the satellite, thereby reducing the gradient across the optical elements. As mentioned before, gradients are not as serious an optical problem at 10.6 microns as in the visible spectrum.

2.1.1.3 IMAGE MOTION COMPENSATOR

After the telescope collects and focuses the received energy, the energy passes through a negative lens that also acts as a filter. The negative lens collimates the converging telescope rays into a pencil-thin parallel beam which is then directed into the image-motion compensator, or fine-pointing mechanism. Selective mirror coatings and lens filter materials eliminate the necessity to

OPTICAL SURFACE COATINGS

Reflectance of Al-SiO-Al-SiO filter mirror as a function of wavelength. Layer deposition controlled at 550 mμ

Layer arrangement in Al-SiO-Al-SiO filter mirror

Reflectance of Al-SiO Filter mirror as a function of wavelength. Layer deposition controlled 0.55μ
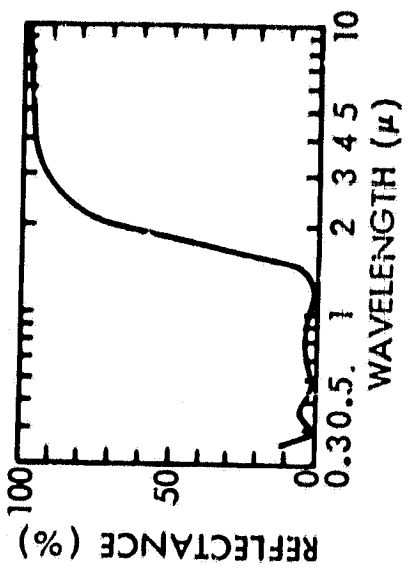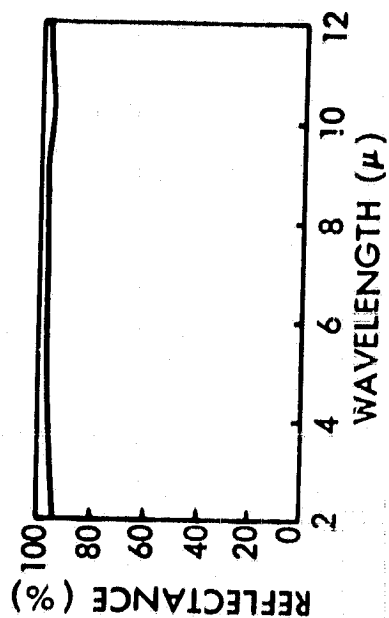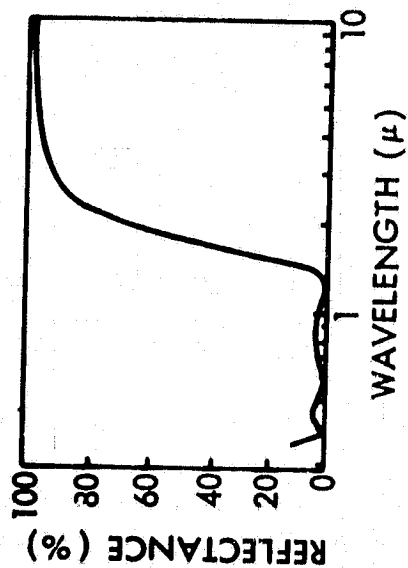
Figure 2-4. Reflectance properties of infrared coatings

shutter the system from direct sunlight. At 10.6 microns, the sun's energy is decreased four orders of magnitude from the value at the peak of its spectrum. In any of the planned experiments, the time the sun can be in the field of view of the optical system is of very short duration.

The image motion compensator corrects instabilities in satellite pointing. It is assumed in this proposal that the satellite is Earth-oriented and stabilized by a 3-axis inertial-wheel control system to a specified accuracy of ± 0.1 degree with a jitter rate of 0.0003 degrees per second. This can, however, be relaxed considerably without harming the performance of the laser experiment. The required pointing accuracy of the optical system, on the other hand, is approximately ± 0.0015 degree, representing a dynamic control range of only 72:1. Satellite operational fine-guidance systems operate at dynamic range levels as high as 200:1 (200 resolution elements). To implement fine control of optical beams over a relatively narrow field-of-view, new operational techniques are being developed to supplement older, well proven techniques, such as the galvanometer movement that can steer optical beams very precisely without causing large bearing-supported components to be moved.

One technique the Optical Systems Branch employs for optical beam steering is based on small piezoelectric bender bimorphs as the active deflection elements.[4] A simplified diagram of the optical beam-steerer is shown in Figure 2-5. By moving one mirror in a direction orthogonal to the movement of the other mirror, an infinite number of beam direction can be obtained. The number is limited only by the resolution of the system. For initial beam acquisition, the course beam pointing mechanism is commanded to point to the satellite or ground station to which communication is to be established. The laser transmitter is turned on and modulated with a single tone. To ensure that the target is within the radiation pattern, the transmitter is operated in a wide divergence mode by either bypassing the main optics or employing a "Zoom" lens arrangement. Even though the beam must be widened considerably, (the required amount of widening is controlled by the attitude stability of the transmitting and target satellites) the power level at the target satellite will be more than ample for heterodyne detection of the narrow bandwidth acquisition signal. The ultimate sensitivity limit for heterodyne detection is nominally 10^{-20} watts per cycle of bandwidth.

The energy entering the optical system on the target satellite (Figure 2-6) is focused somewhere in the focal plane of the 25-cm Cassegrain telescope. Note that the radiation falling on the 10.6 micron detector at any instant will be arriving from a narrow cone corresponding to the diffraction limit of the 25-cm telescope (± 0.0025 degree). However, the image plane can be scanned sequentially by the image motion compensator bimorphs so that the detector samples a much larger angular field, see Figure 2-7.

Figure 2-5. Image-motion compensator beam steerer configuration

In order for acquisition to occur, the beam must dwell long enough on one of the error sensor detectors for the system to recognize the received signal and respond by stopping the scanning operation and initiating the procedure to center the beam on the error sensor. Since the detectors have a very short response time (on the order of tens of nanoseconds) and the associated recognition

Figure 2-6. Initial acquisition wide beam transmission

TARGET
SYNCHRONOUS SATELLITE

20 SEC

OPTICAL SYSTEM
FIELD-OF-VIEW

DETECTOR INSTANTANEOUS
FIELD-OF-VIEW

SYNCHRONOUS
SATELLITE
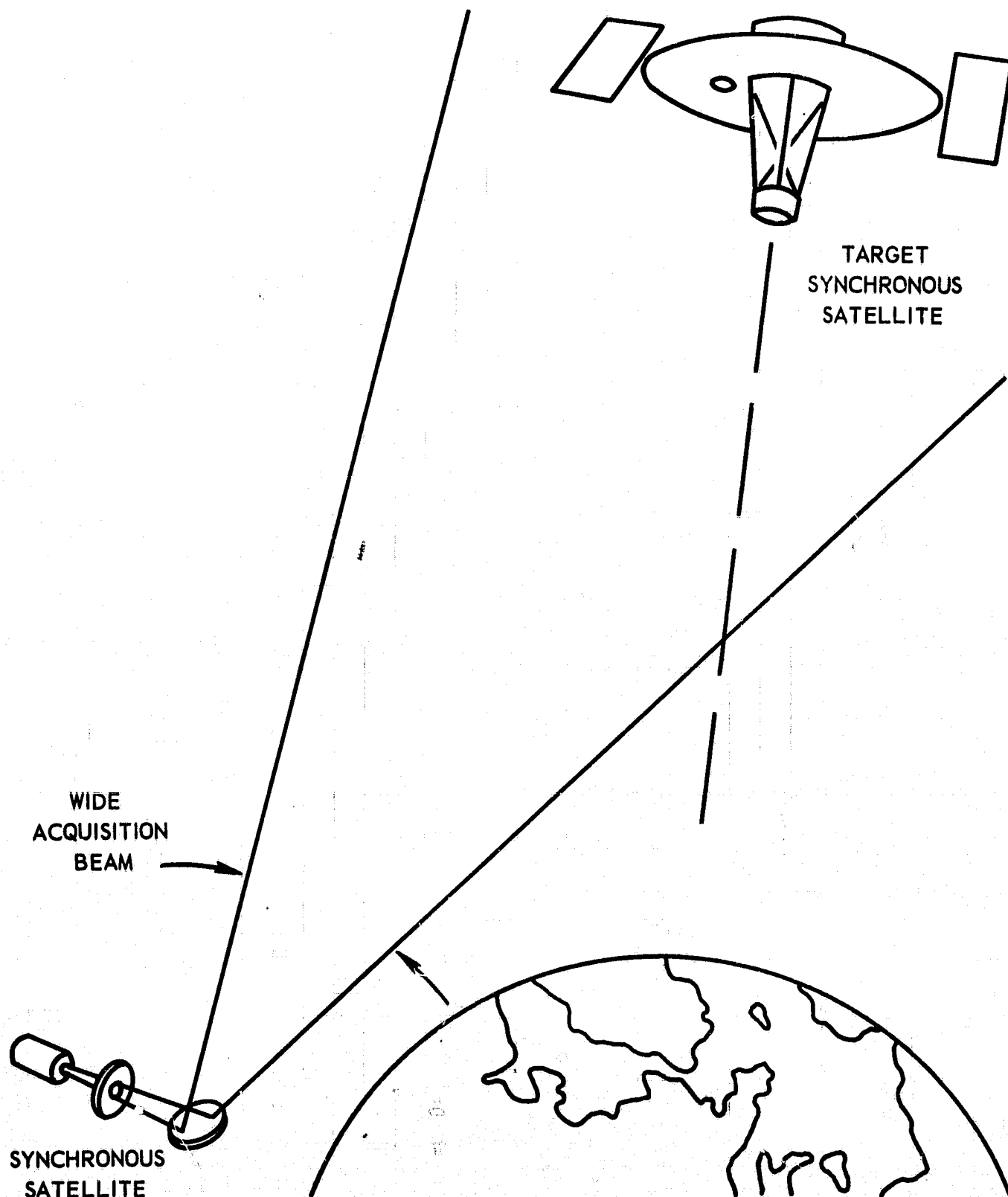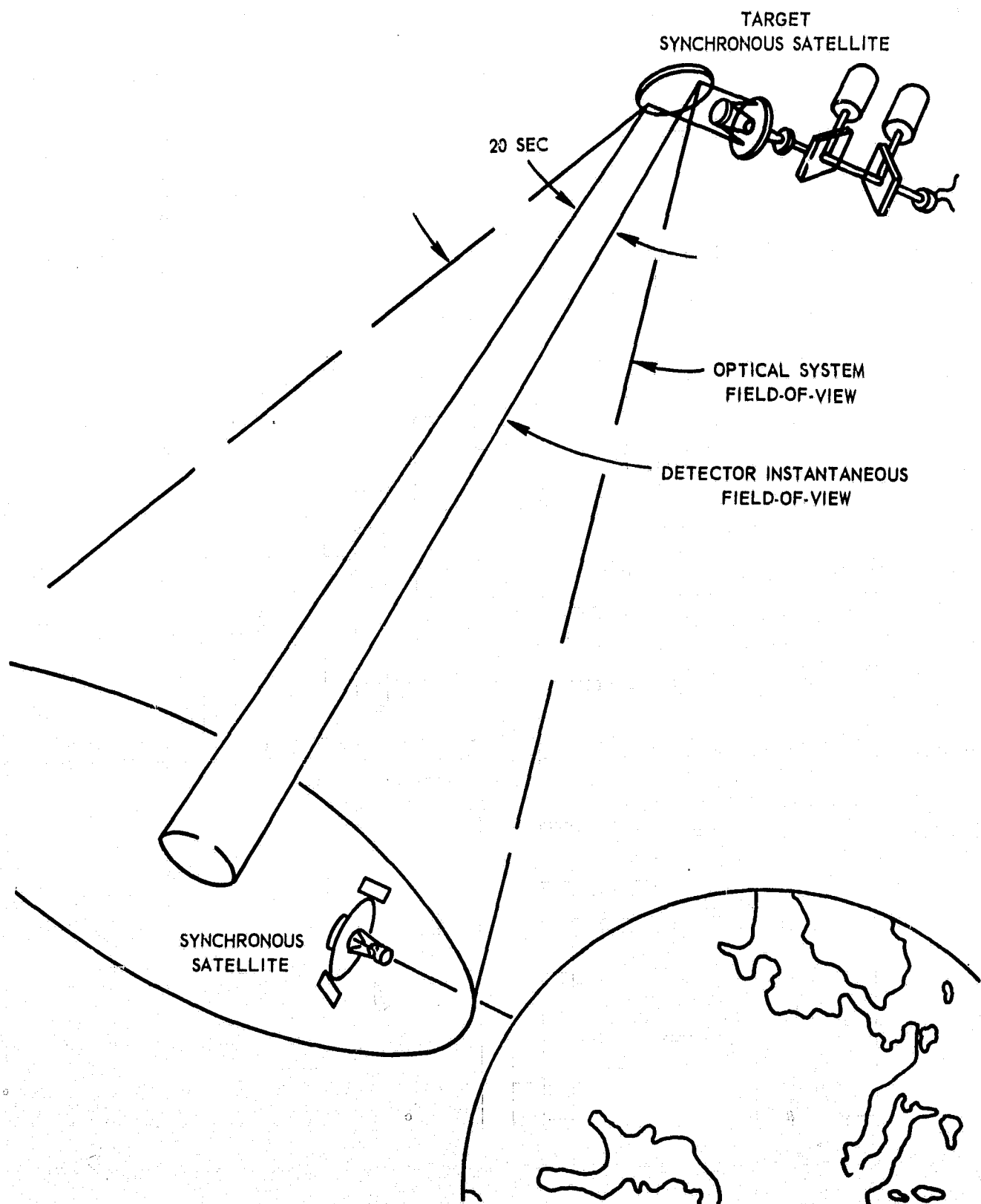
Figure 2-7. Search scan-acquisition operation

electronics can be designed to have a very fast response, the primary limitation on acquisition time appears to be the performance of the image motion compensator. The currently available image motion compensator, utilizing piezoelectric bender bimorphs, is capable of being driven at a 5 KHz rate. This rate is sufficiently fast to permit spiral scan over any reasonable, or plausible, field-of-view in a few tens of milliseconds.

At a typical satellite drift rate of 0.003°/sec. (10.8 arc sec./sec.) several complete field scans would be accomplished before the target could drift out of the field (assuming the target to be at the edge of the field). Therefore, the probability of target acquisition during the "first try" is quite high.

Once the target synchronous satellite has acquired the acquisition beam, an error signal is generated to maintain acquisition. This can be done in several ways, to give a few examples: by a rotating chopper wheel or optical wedge, nutating mirrors, or with a multiple detector arrangement as in the present proposal.

Since the laser transmitter is boresighted to the optical axis, turning on the transmitter on the target satellite will transmit a beam directly to the satellite transmitting the wide acquisition beam, i.e. the beacon. The scan operation is then repeated on the first satellite until the beam from the target satellite is acquired. At that time the first satellite's laser transmitter is changed from the wide beam acquisition mode of operation to narrow beam communication mode and the beam divergence is reduced to 20 arc seconds. The communication link has then been established and both ends of the link are in an autotrack mode, see Figure 2-8.

The present image motion compensator (Figure 2-9) provides a performance capability exceeding the requirements for the laser optical communication experiment.

2.1.2 LASER SUBSYSTEM

Two lasers will be used in the spacecraft package: a 100-mw local oscillator and a 2.4 watt transmitter. The transmitter beam is directed through an external modulator to provide the 100 MHz of modulation bandwidth. A functional diagram of the lasers and the laser control electronics is shown in Figure 2-10.

The primary design consideration in the transmitter and local oscillator laser is that of frequency stability. This problem is being addressed in the ATS-F Laser Communication Experiment and the NASA-ERC development of a space-qualified CO_2 laser. The lasers for the Advanced Laser Communication Experiment
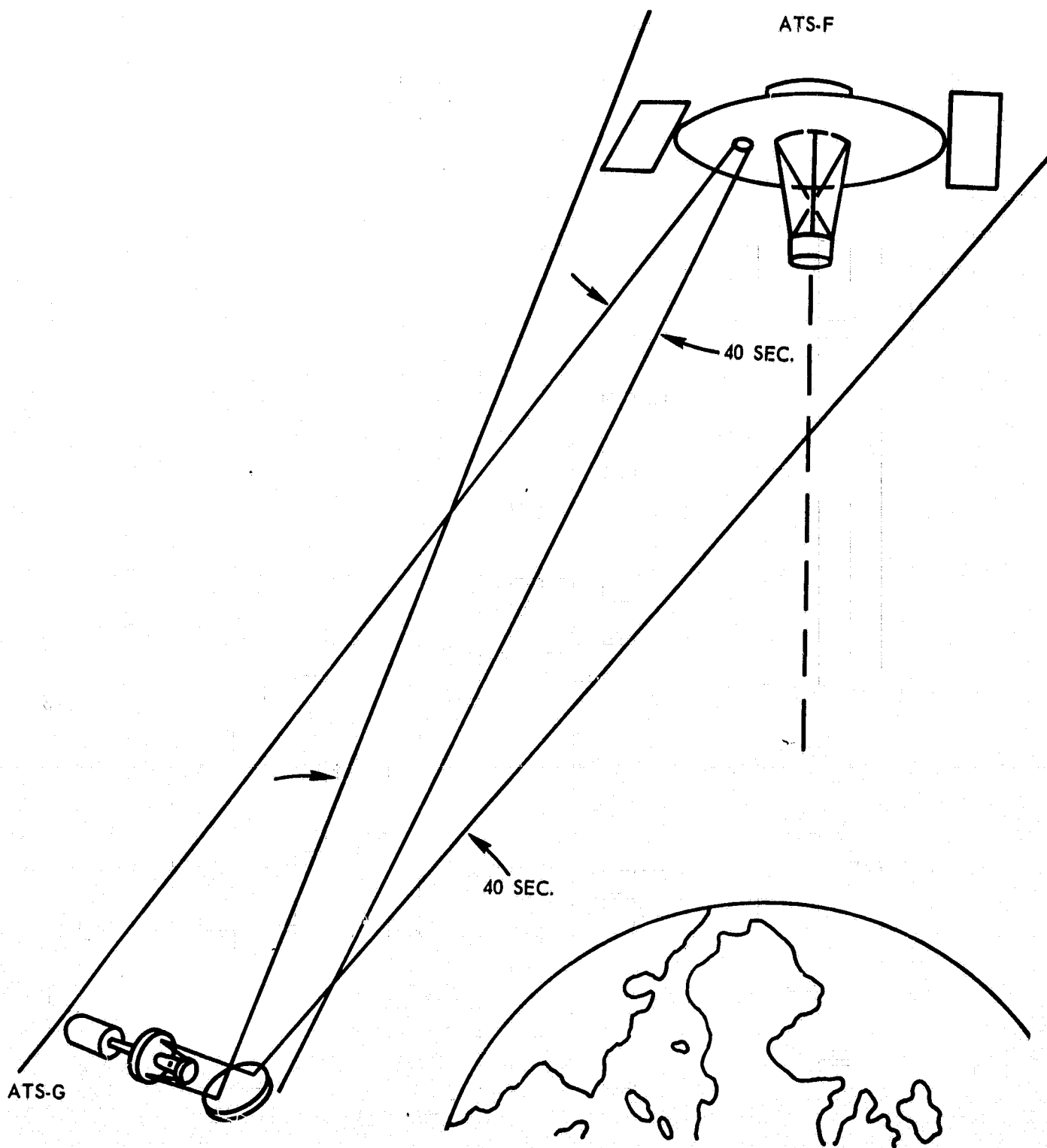
ATS-F

40 SEC.

40 SEC.

ATS-G

Figure 2-8. Communication link established-both systems transmitting narrow beam
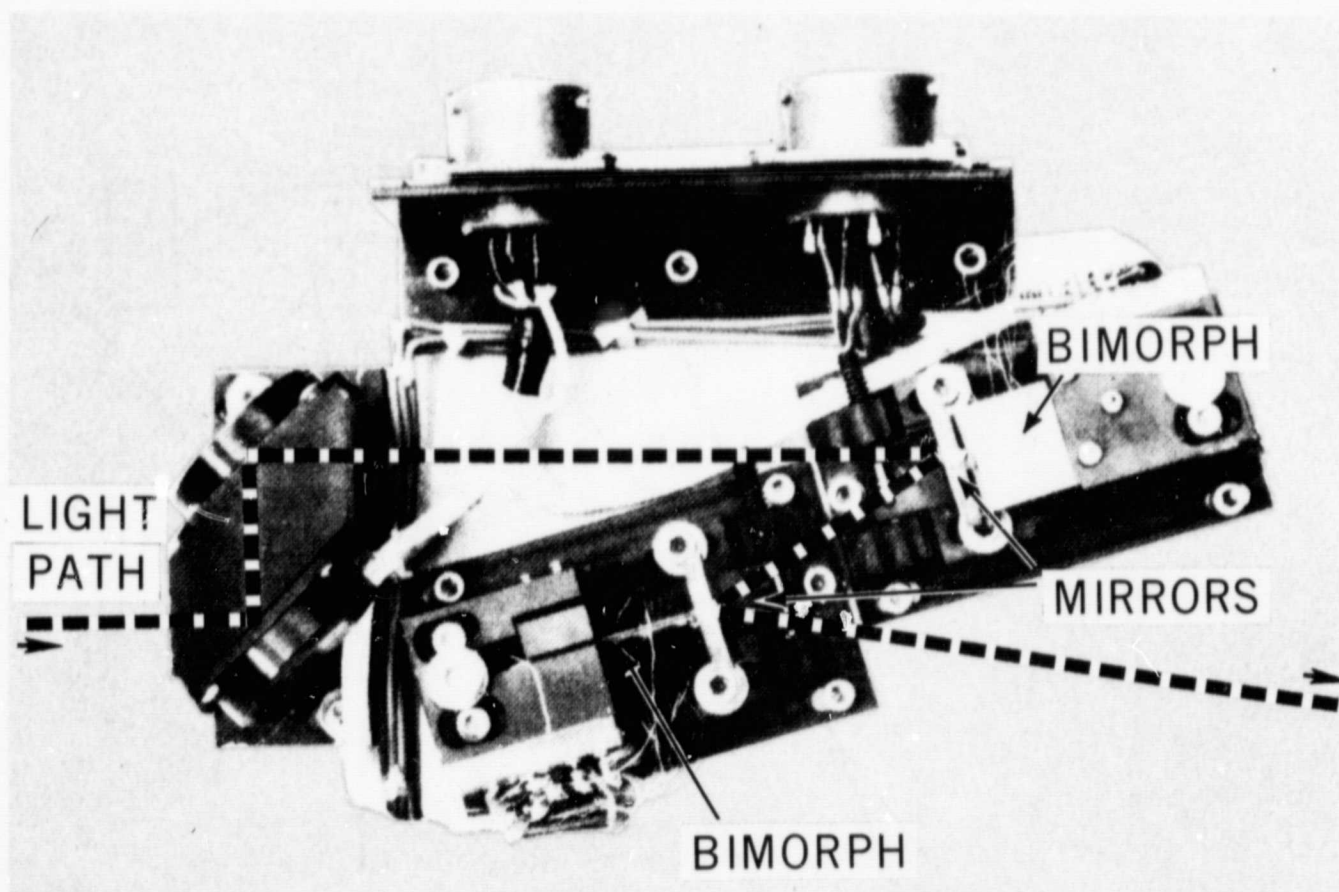
2-15

Figure 2-9. Image-motion compensator using bender bimorphs

will be a direct outgrowth of this work. One laser mirror will be mounted on a piezoelectric stack to permit fine tuning of the laser frequency. It may be desirable to connect the piezoelectric stack into an automatic frequency control servoloop in order to maintain the required stability. The question of active versus passive stabilization will be thoroughly investigated in this program.

The modulator will, in all likelihood, be an external modulator, unless pressure broadening or isotopic additives can be used to broaden the 50 MHz Doppler-broadened spectral line of the carbon dioxide laser. Several alternative modulation schemes must be carefully examined in this program to determine the optimum technique. Among them are: external electro-optic, optical-induced free carrier, and the use of current-modulated injection lasers operating at 10.6 microns.

2.1.3 DETECTOR SUBSYSTEM

2.1.3.1 SIGNAL INFORMATION DETECTOR

The optical subsystem directs the incoming infrared signal to the signal information detector and error sensor. Although the two are combined in a single
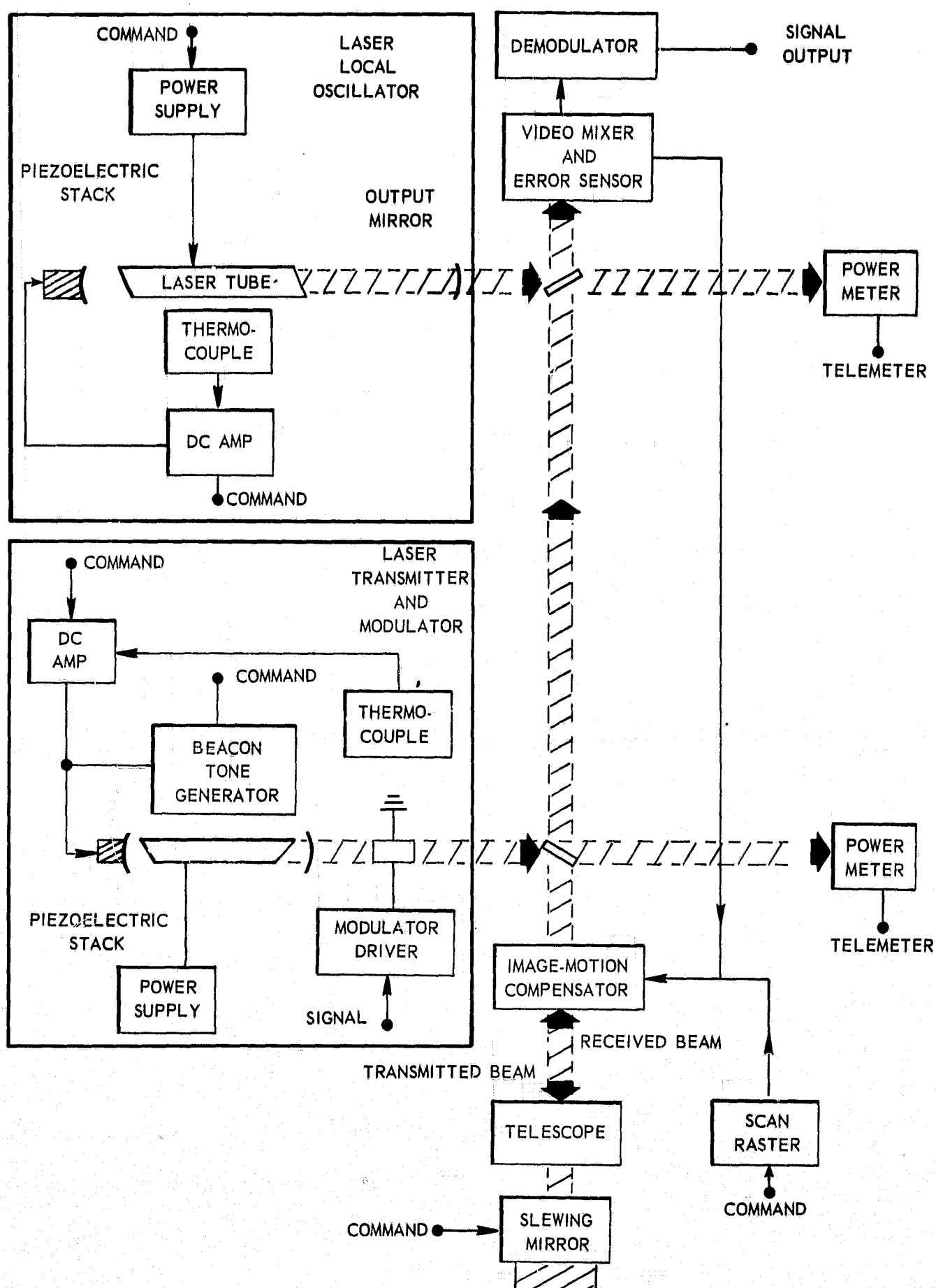
Figure 2-10. Functional diagram of lasers and laser control electronics

unit, they will be discussed separately. The use of coherent heterodyne detection is proposed for this experiment because it is superior by six orders of magnitude to direct envelope detection in sensitivity and i' s ability to discriminate against background. Heterodyne detection involves the coherent mixing of the incoming laser signal with the local oscillator in a square-law photodetector. The emergence of coherent laser technology has now made possible the performance of this function, which is analogous to radio-frequency techniques. The ultimate sensitivity limit for heterodyne detection, termed the quantum limit, is 2hfB or nominally 10^{-20} watt per cycle of bandwidth. Recent measurements by Arams,[5] Teich,[6] and Mocker[7] have shown that sensitivities within a factor of 2 of the quantum limit are attainable, see Figure 2-11.

The detector used will be either mercury cadmium telluride (HgCdTe), lead tin telluride (PbSnTe), or one of the recently developed metal-to-metal point contact diodes.[8] Each of these has the capability of operating at elevated
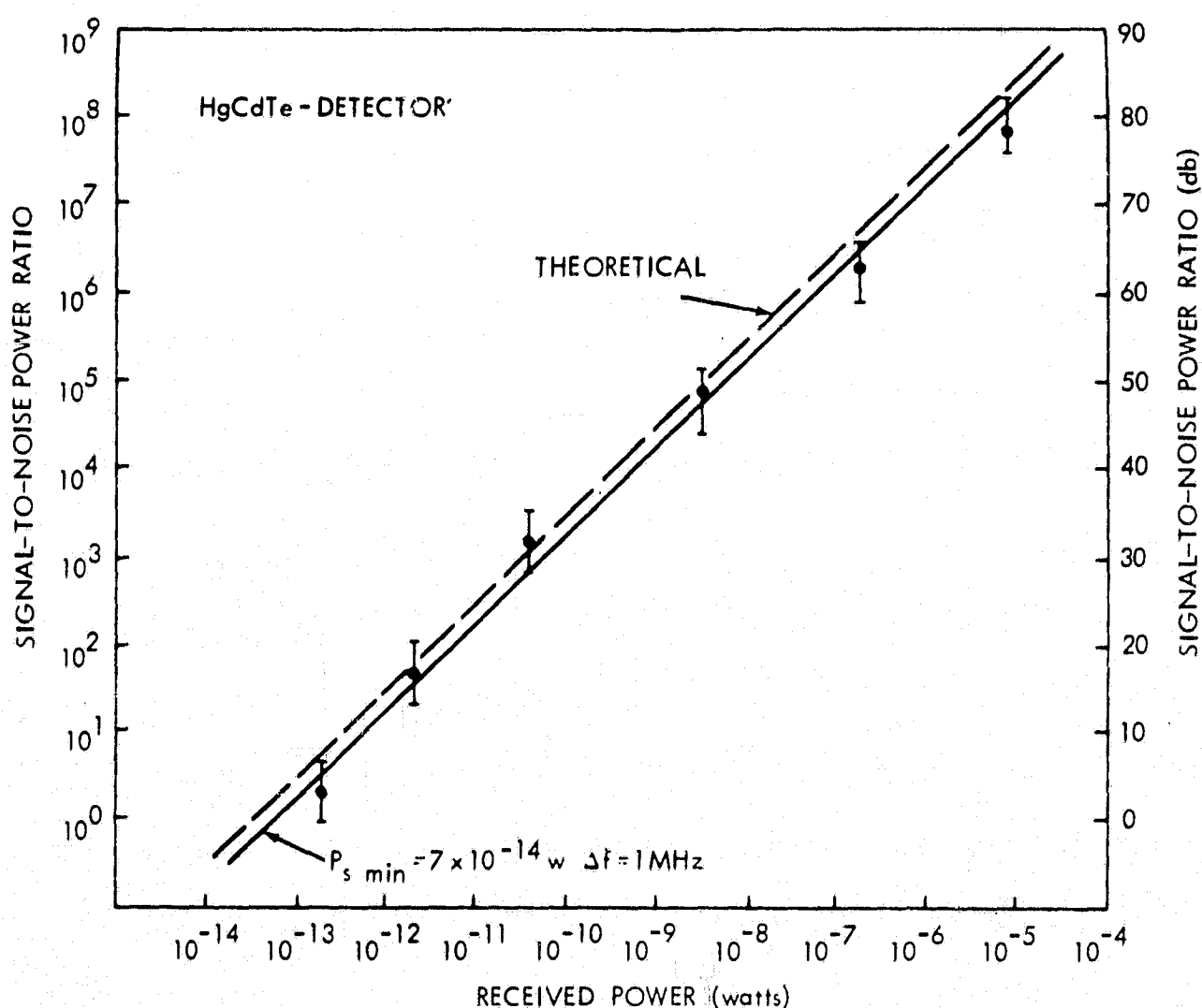

Figure 2-11. Far-infrared mixer sensitivity measurements made on a HgCdTe element

temperatures in comparison to the conventional photoconductive detectors that are used at 10.6 microns. The first two can be operated at temperatures in excess of 100°K and the last may permit room temperature operation. A major part of the development in this program will be the optimization of the infrared mixer.

The ability to obtain satisfactory performance at elevated temperatures, 100°K in two cases or room temperature in the third, allows the use of radiative coolers or, perhaps, no cooler at all, to obtain the required operating temperature for the detector. Radiative coolers require no power, are very light weight, and have an essentially unlimited lifetime. The effect of operating temperature upon the detectivity of a HgCdTe detector is shown in Figure 2-12.
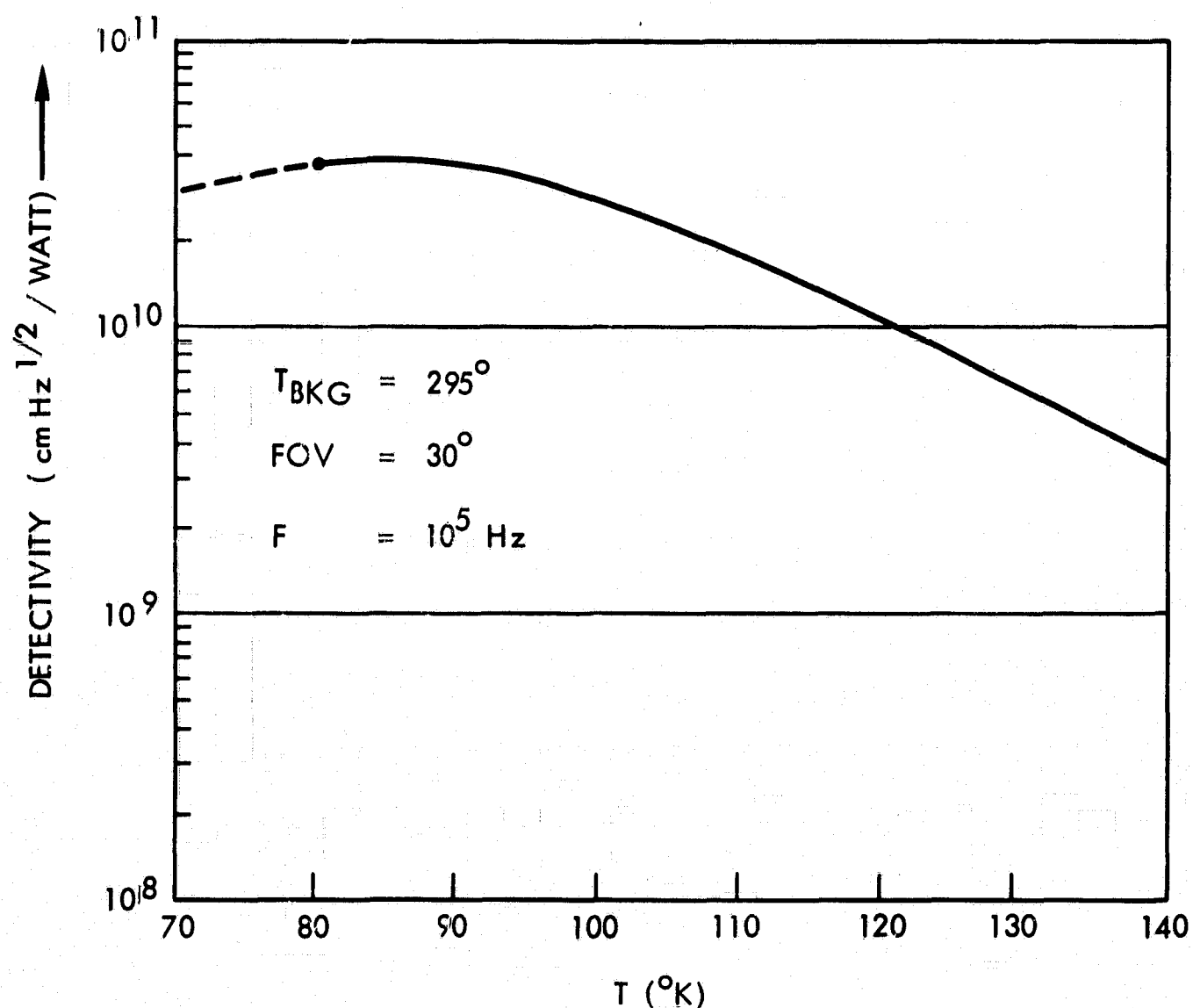

Figure 2-12. The effect to operating temperature on detectivity of an IR mixer

2.1.3.2 FINE BEAM-POINTING ERROR SENSOR

The fine beam pointing error sensor is a five element detector matrix made up of a four element quadrant error sensor with a signal detector in the center of the quadrant array. When the incoming beam is centered on the signal detector, each element in the quadrant array receives an equal signal and no error signals are generated. If, however, an imbalance of energy occurs, an error signal results which directs the image motion compensator to recenter the image.

The fine beam-pointing error sensor provides the servo error signals necessary to operate the image-motion compensator that controls the direction of transmitted and received rays. Sensor operation can be divided into two modes: acquisition and tracking. The acquisition mode starts when the image-motion compensator initiates a scan program; it terminates when the error sensor registers acquisition of a signal and sends a command to the scan program to halt the scanning operation. The tracking mode starts with the acquisition of a signal. After acquisition has been registered, the image of the incoming laser beam is automatically centered on the error sensor. Subsequent drifts in the image position result in azimuth and elevation error voltages that cause the image motion compensator to recenter the image.

As in the signal information detector, heterodyne detection will be used for maximum sensitivity. The four detectors of the error sensor are followed by identical sequences of preamplifier, filter, and RF detector, see Figures 2-13 and 2-14. Since it is presumed that the incoming beam direction is uncertain over a range of 720 arc-seconds (± 0.1 degree), the diffraction-limited spot size on the detector array is 20 arc-seconds, producing 36 resolution elements across the focal plane. Therefore, if the detector dimensions are matched to the resolution element, the exact spot location could be determined if an array of 36 by 36 detector elements were placed in the focal plane. To avoid the complexity, and impracticality, of such a system, a two by two array is employed in conjunction with a scanning system that uses the image motion compensator.

The scanning programmer causes the image-motion compensator to begin a spiral scan of the field of view of the optical system. The dwell time at each position is matched to the reciprocal of the tracking bandwidth and is long enough to permit acquisition when the beam strikes a detector element. The experiment design will result in typical acquisition times of much less than one minute.
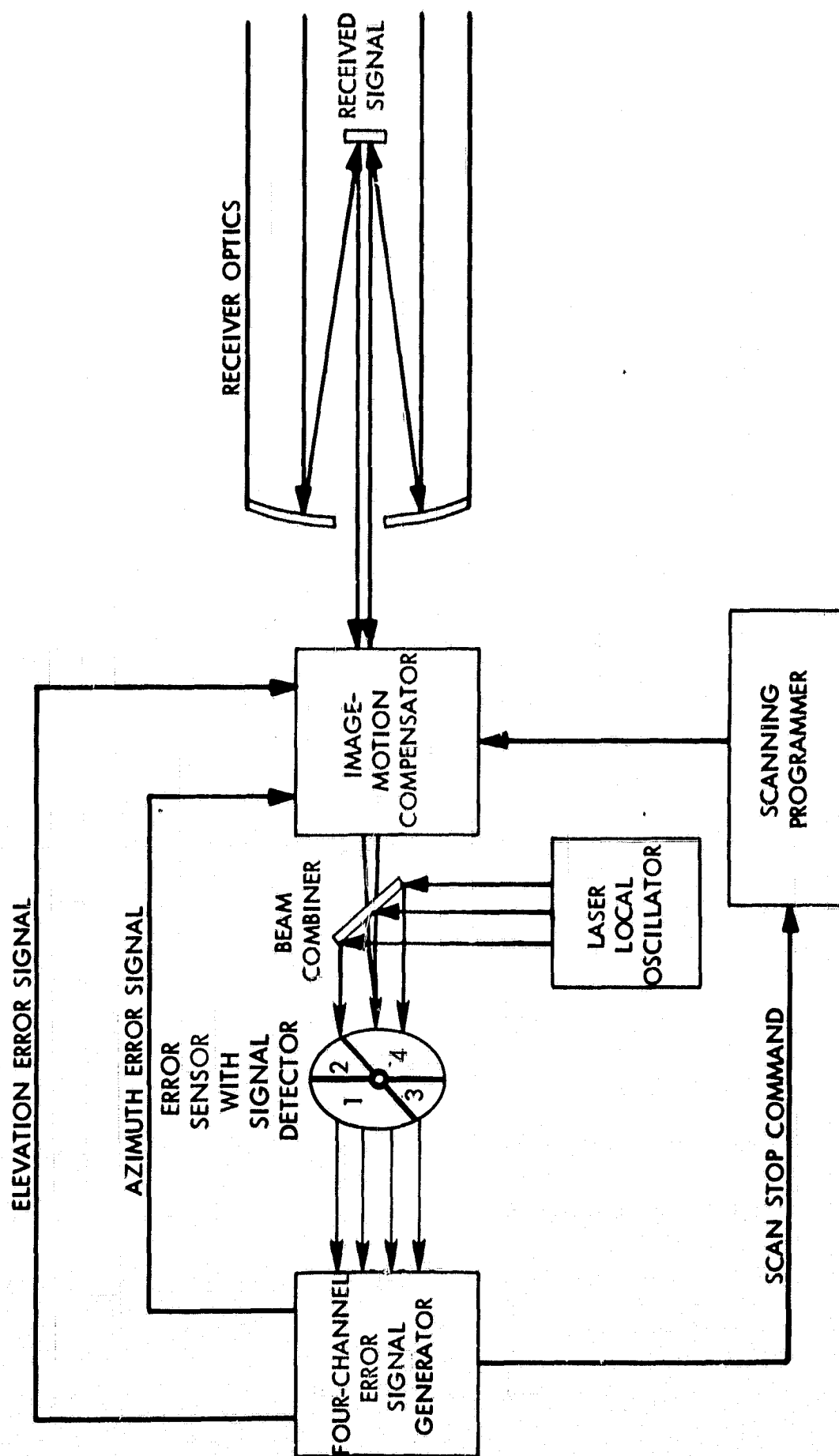
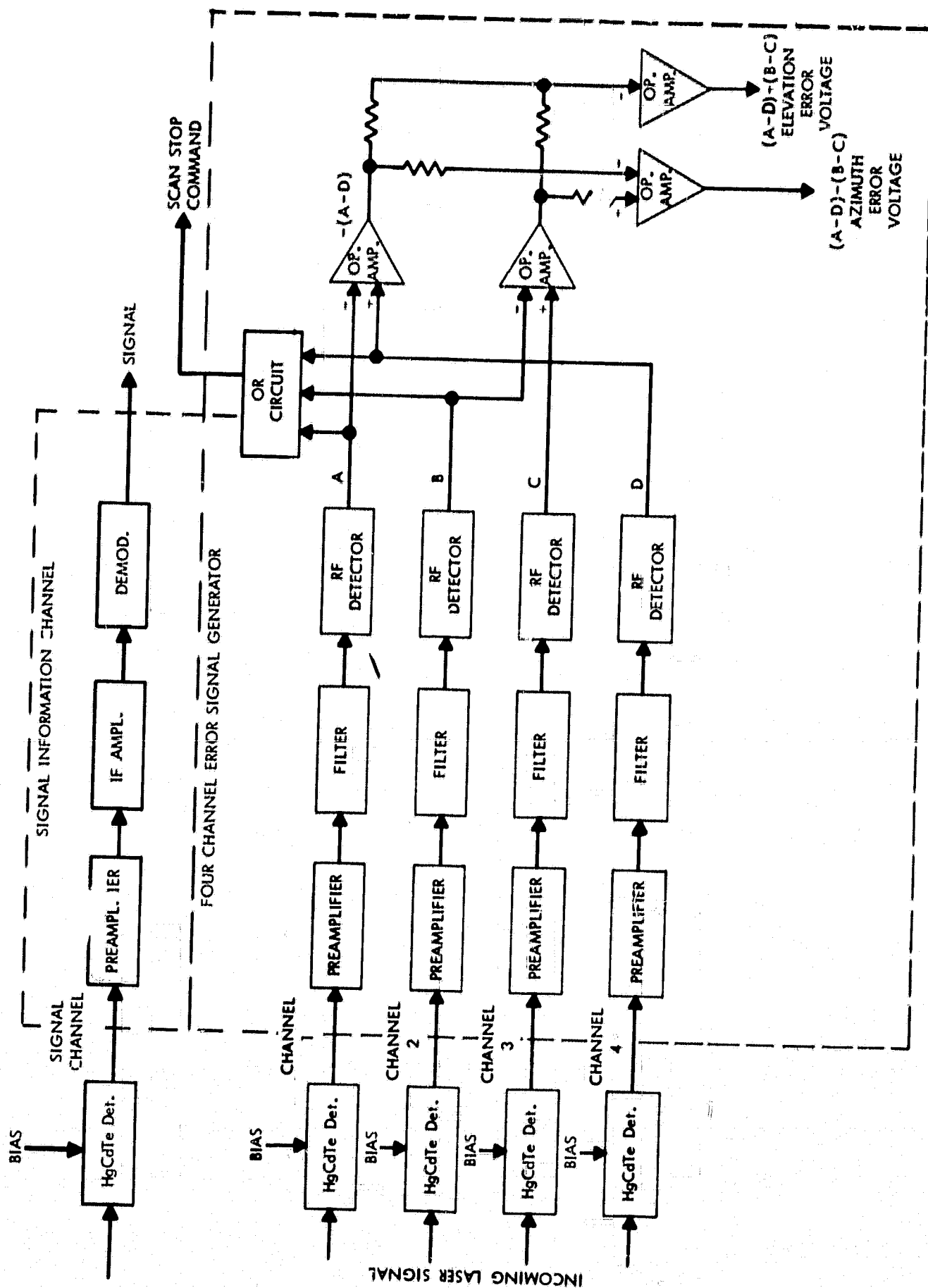Figure 2-13. Block diagram of fine beam-pointing control

Figure 2-14. Beam compensator error-sensing circuit

2.2 SYNCHRONOUS SATELLITE TO LOW-ALTITUDE SATELLITE COMMUNICATION SYSTEM

The system employed to establish communication between the synchronous satellite and the low-altitude satellite is fundamentally the same as the one employed for synchronous to synchronous satellite communication. There are two important differences: first, the tracking and acquisition sequence is somewhat more demanding, but not greatly so, and, second, the detector and following electronics must be capable of handling the high Doppler frequency shifts that will occur in the link. Each of these will be discussed briefly below.

The differences in the tracking and acquisition sequence are primarily ones of increasing the angular tracking rate capability and increasing the maximum angular travel in the North-South direction. Neither of these factors appears to be a serious problem. The acquisition technique to be employed follows the same sequence as that described in the previous section. The low-altitude satellite will be illuminated by a broadened beam from the synchronous satellite. The broadened beam will be acquired by a receiver search scan operation. A narrow beam from the low-altitude satellite will then be directed at the synchronous satellite which will proceed to narrow its transmitted beam. One of the major facets of this operation to be investigated will be that of "hand-over" of communication with a low-altitude satellite from one synchronous satellite to another.

Another major area of development will be the production of Doppler tracking loops to follow the wideband "front-end" of the laser receiver. These loops will track the changing Doppler shift and allow the noise bandwidth of the receiver to be narrowed to approximately the same bandwidth as the signal information. Without such capability no communication would be possible. In order to estimate the difficulty of the problem, an essentially simple analysis has been carried out. For illustration, assume that communication is to be established between a synchronous satellite and a low-altitude satellite of the Nimbus category. The Nimbus satellites are in a 107 minute, polar orbit at an altitude of nominally 600 nautical miles. The geometry of the problem is shown in Figures 2-15 and 2-16. It is assumed that the synchronous satellite is positioned over the Equator. Figure 2-15 shows the simplest geometrical situation, but the worst case situation for the Doppler shift. In Figure 2-15 it is assumed that the low-altitude satellite in polar orbit passes directly underneath the synchronous satellite. The angle Ω is the elevation angle of the low-altitude satellite with respect to the equatorial plane; positive values of Ω are in the Northern Hemisphere and negative values are in the Southern Hemisphere. As the satellite passes over the South Pole the magnitude of the Doppler shift increases until it peaks at $\Omega = -79°$. The Doppler shift decreases to zero as the satellite moves northward across the Equator and then begins to increase in the opposite direction as the satellite proceeds toward
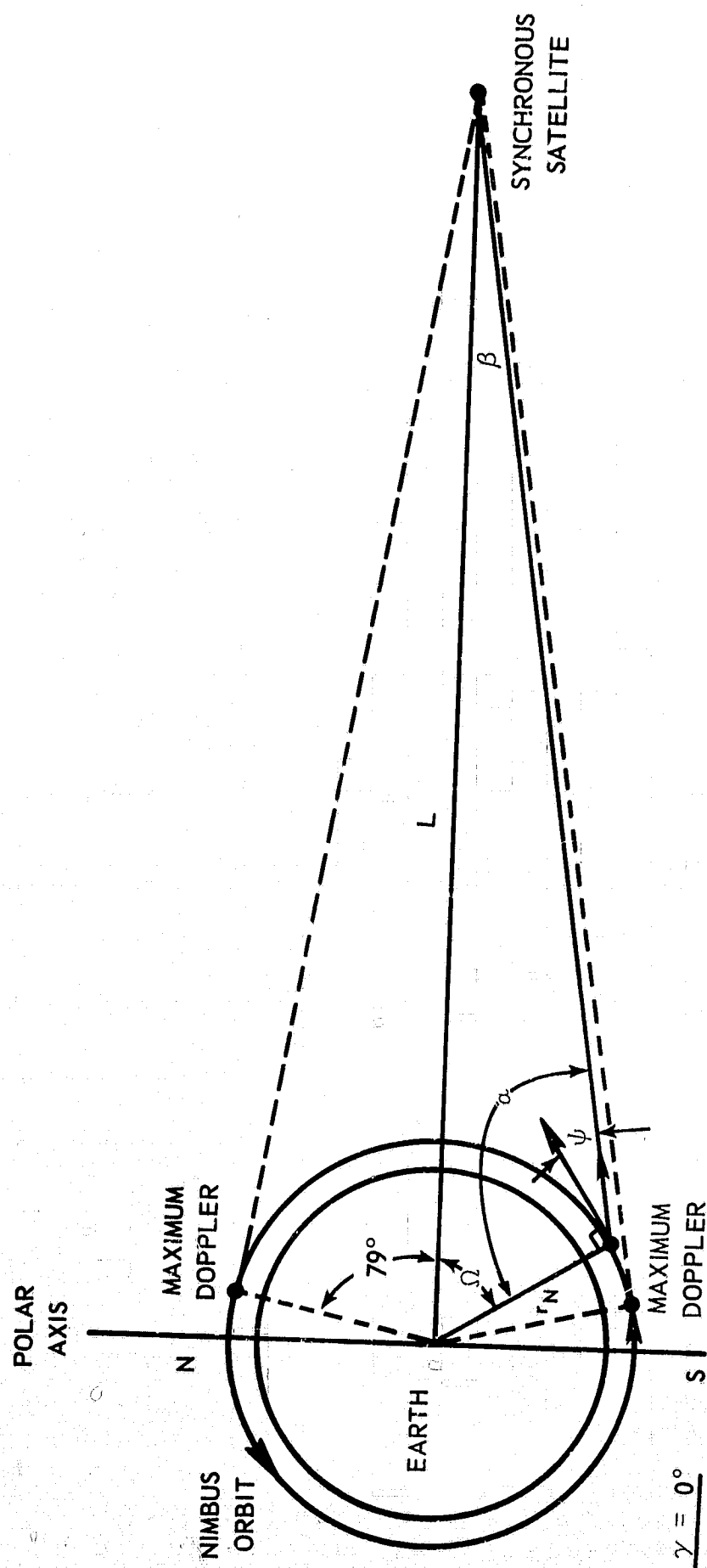
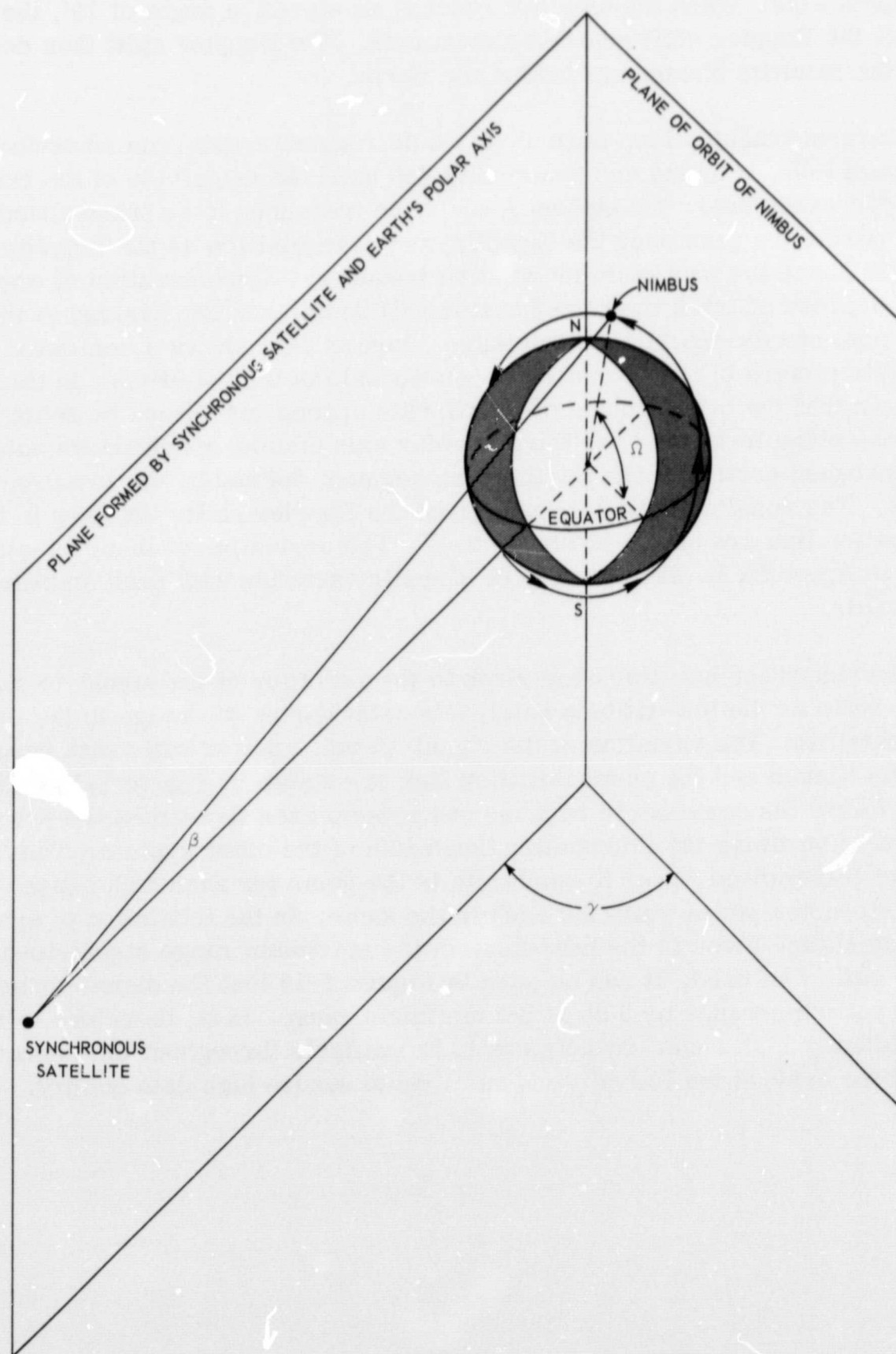Figure 2-15. Geometry for computation of Doppler frequency shift with $\gamma = 0°$

Figure 2-16. Geometry for computation of Doppler frequency shift with $\gamma \neq 0°$

the North Pole. When the satellite reaches an elevation angle of 79°, the magnitude of the Doppler shift reaches a maximum. The Doppler shift then decreases until the satellite disappears behind the Earth.

Current tracking loop technology would require acquisition somewhere above the South Pole, tracking and communication until the magnitude of the Doppler shift decreases below the highest modulation frequency to be transmitted, loss of track during the pass over the Equator, and reacquisition as the Doppler shift increases above the maximum modulation frequency. Consideration of ways to avoid the loss of track over the Equator will be an area emphasized in the development of this experimental package. Figure 2-16 shows a somewhat more complete picture of the geometrical relationship of the satellites. In this case it is shown that the orbital plane of the Nimbus spacecraft differs by some angle, γ, from the plane formed by the Earth's polar axis and the synchronous satellite. The unshaded portion of the Earth is the segment defined by the two intersecting planes. The results of the computation of the Doppler shifts involved in the communication link are shown in Figure 2-17. The derivation of these results is given in Appendix B. It is seen to be a cyclic variation with peak amplitudes of ±1.35 GHz.

Consideration has also been given to the variation of the signal-to-noise power ratio as the low-altitude satellite's orbit varies the range to the synchronous satellite. The variation of the signal-to-noise power ratio with range for both the beacon and the communication link are shown in Figure 2-18. The two cases follow the same curve because one system uses five times the power to transmit five times the information bandwidth of the other system. Thus, the ratio of transmitted power to bandwidth is the same for each and, hence, the signal-to-noise power ratio for each is the same. In the tabulation of system characteristics given in the introduction, the maximum range signal-to-noise power ratio was used. It can be seen in Figure 2-18 that the signal-to-noise power ratio increases by 3 db at the minimum range. It is, therefore, clear that a sufficiently high signal-to-noise ratio is available throughout the visible portion of the orbit of the low-altitude satellite to assure high data quality.

Figure 2-17. Doppler shift as a function of elevation angle, Ω, and inclination angle, γ

$$\left(\frac{S}{N}\right)_P = \frac{\eta \, T_R \, P_T \, G_T \, G_R \, \lambda^3}{2hc \, B \, (4 \pi R)^2}$$

$\eta = 0.5$

$T_R = 0.1$

$P_T = 1.1$ w. (COMMUNICATIONS)
0.22 w. (BEACON)

$G_T = 92.4$ db (COMMUNICATIONS)
98.5 db (BEACON)

$G_R = 98.5$ db (COMMUNICATIONS)
92.4 db (BEACON)

$\lambda = 10.6 \, \mu$

$B = 5$ MHz (COMMUNICATIONS)
1 MHz (BEACON)

$h = 6.63 \times 10^{-34}$ JOULE·SEC.

$c = 3 \times 10^8$ M/SEC.

Figure 2-18. Variation of (S/N)$_P$ with range

2-28

3. DESCRIPTION OF EXPERIMENT

The experimental package described in this document will be the culmination of several years of developmental effort. The initial work is envisioned to be a three year program that will result in the production of a breadboard model of the entire communication system.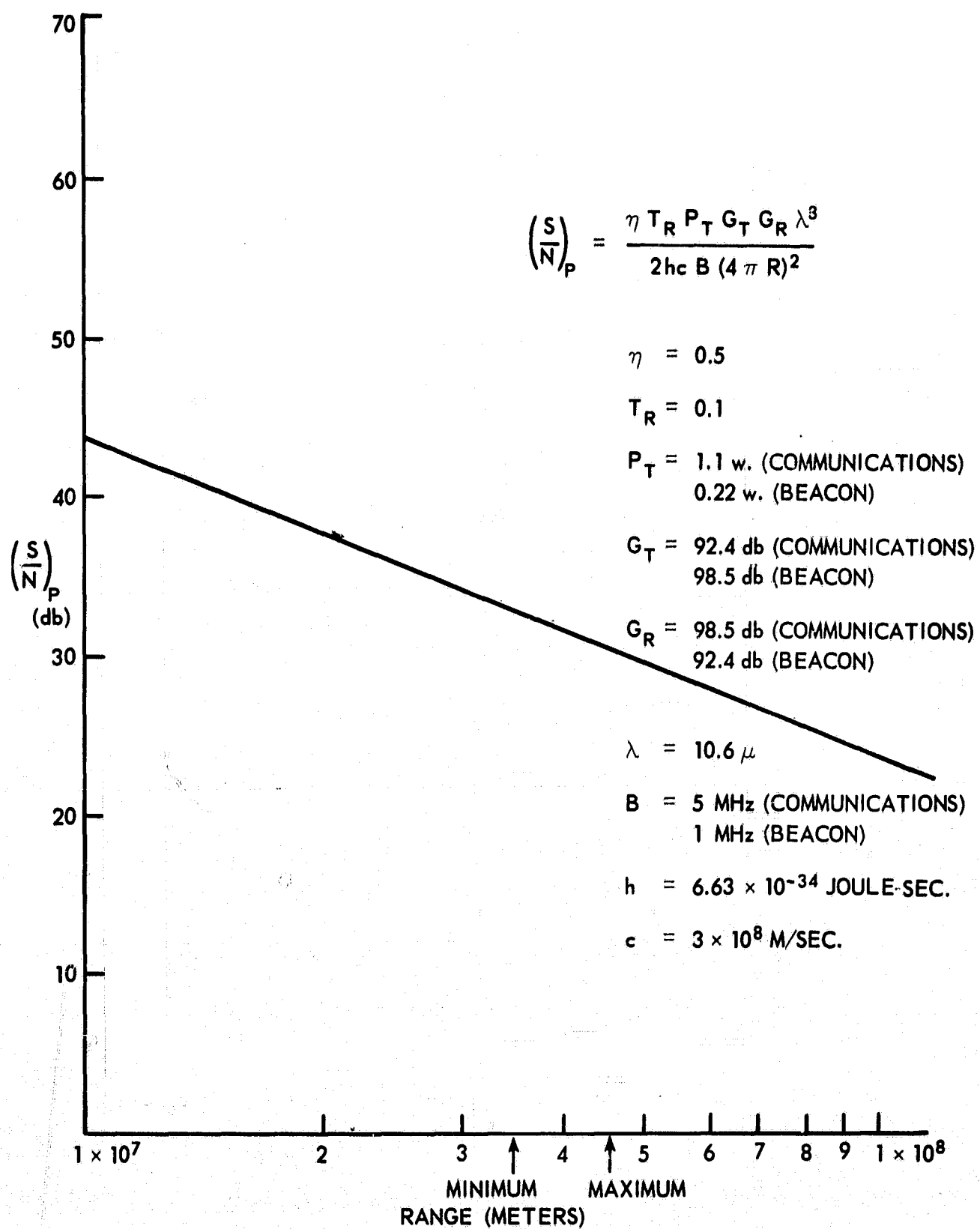 This breadboard will be able to perform all of the tasks of the spaceborne system with the exception of withstanding vibration testing and launch. With this effort completed in the middle of 1972, design of the actual flight hardware could be initiated with an expected date of completion sufficiently early for a launch in 1975.

It is assumed that the first launch would be that of a synchronous satellite with both the synchronous-to-synchronous satellite communication equipment and the synchronous-to-low altitude satellite communication equipment on-board. Both communication systems will be designed to have sufficient flexibility in pointing so that they can be directed at selected ground stations. All testing and experimentation carried out during the initial phase of the experiment would be with a ground station. Testing and experimentation during this phase would consist of measuring the performance of the communication system and comparing it to the expected performance, measuring the individual performances of the various components of the system, and studying both components and system to see what degradation occurs with use and due to the space environment.

The sequence of the experiment after the initial phase can be varied to suit the availability of appropriate spacecraft. The launching of the first synchronous satellite with the advanced laser communication system on-board will create a facility in space with many capabilities. These capabilities can be used by a wide variety of experimenters for numerous experiments. Communications system studies and atmospheric propagation work are only among the more obvious. Experiments such as accurate determination of spacecraft attitude from the laser tracking servo data and measurement of vibration levels on-board the spacecraft are among others that can be easily implemented. If another synchronous satellite is the next to be launched, the synchronous-to-synchronous link can be implemented. On the other hand, should a low-altitude satellite become available next, a communication link could be established with it. In either case, a variety of cross-strapping techniques could be employed to transmit a signal to the spacecraft via either laser or microwaves and then to cross-strap it to either the laser system or microwave system for the return trip and data analysis. A very few of the possibilities are shown in Figures 3-1, 3-2, and 3-3. Figure 3-1 shows single satellite experiments, Figure 3-2 shows dual satellite experiments, and Figure 3-3 shows tri-satellite experiments.
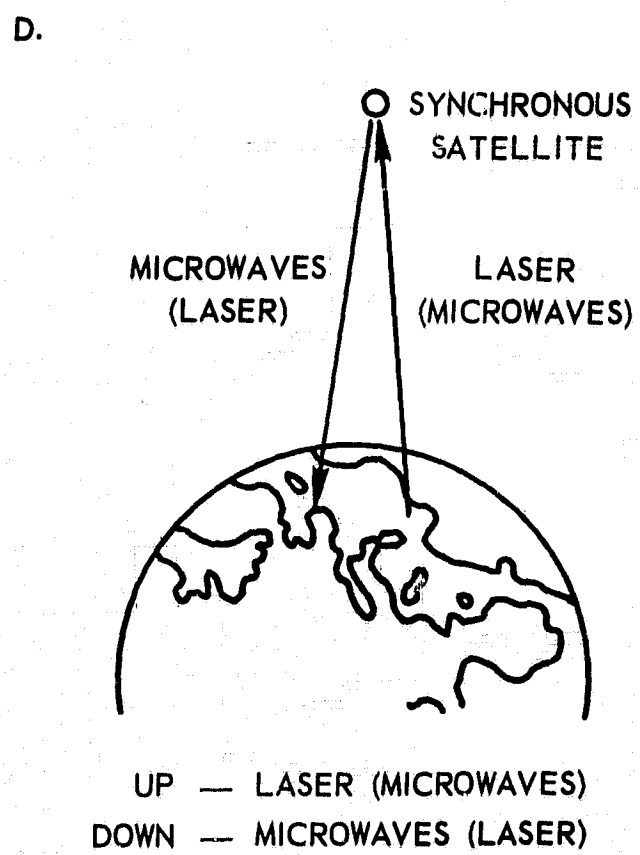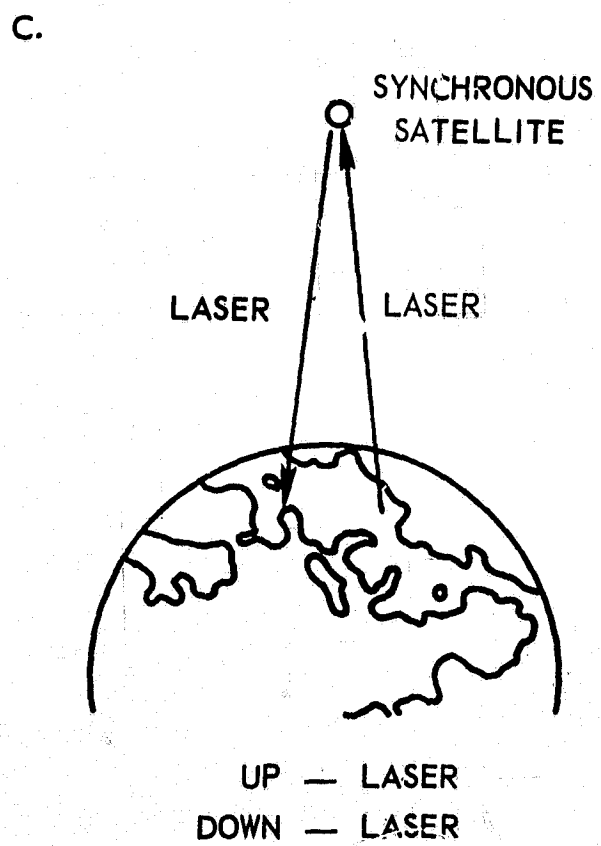
Figure 3-1. Single satellite experiments

Figure 3-2. Dual satellite experiments

A.

SYNCHRONOUS
SATELLITE

LASER

LASER

SYNCHRONOUS
SATELLITE

LASER

LOW-ALTITUDE
SATELLITE

B.

SYNCHRONOUS
SATELLITE

LASER

MICROWAVES

SYNCHRONOUS
SATELLITE

LASER

LOW-ALTITUDE
SATELLITE

Figure 3-3. Tri-satellite experiments

The technology to be developed in this program will permit the most comprehensive possible test of intersatellite communications in general and laser intersatellite communication systems in particular. It provides for the extension and space-qualification of a technology which offers the greatest potential for power- and weight-economical intersatellite communication systems.

4. SPACECRAFT RESTRAINTS

The restraints on the spacecraft imposed by the advanced laser communication experiment are minimal. The satellites must be earth-oriented and have some degree of stabilization. The st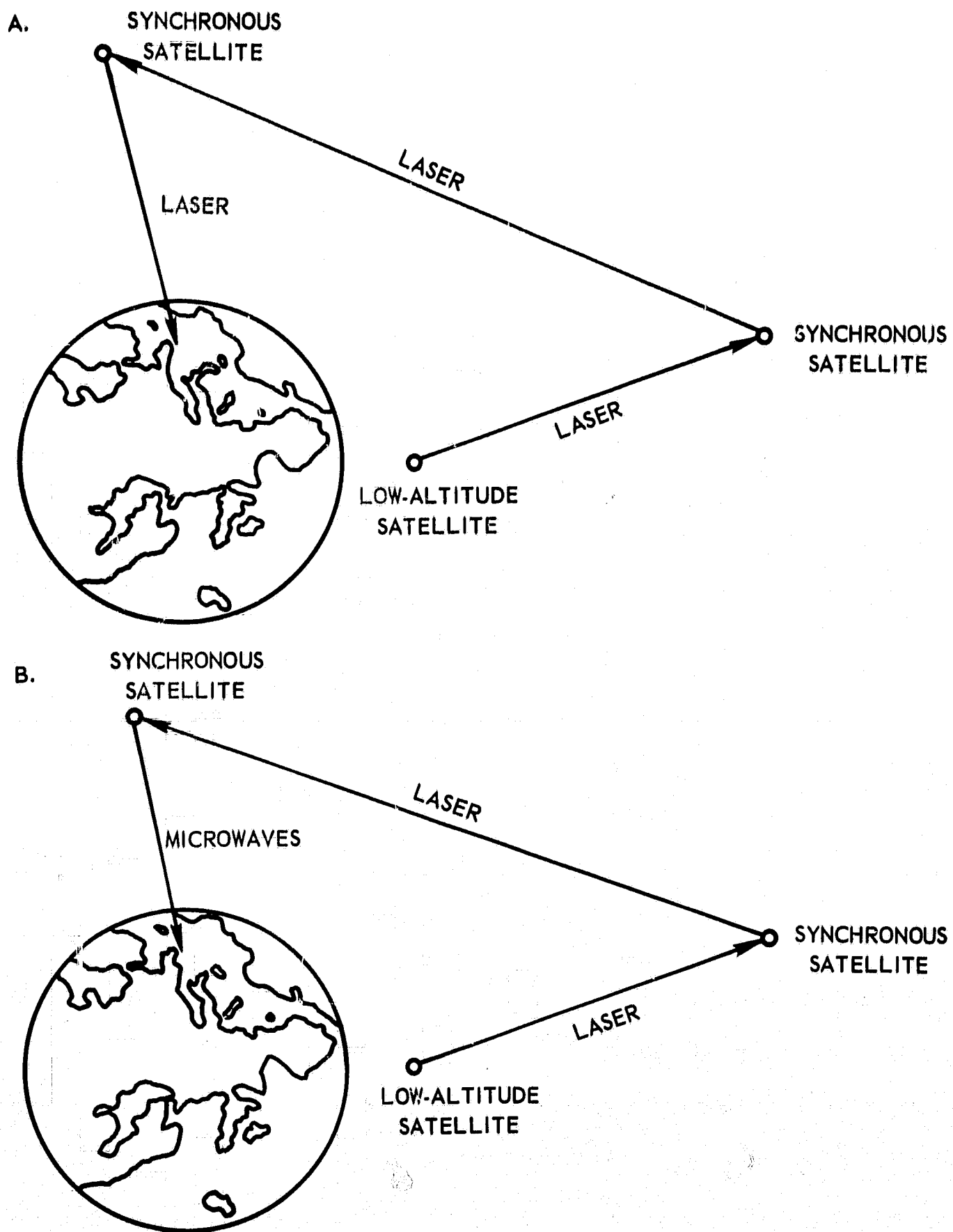abilization of the ATS-F spacecraft which permits pointing of the main antenna to an accuracy of $\pm 0.1°$ and a jitter rate of 0.0003 degrees per second represents an almost ideal platform for a laser communication experiment, but appropriate experiment design would permit the degradation of these parameters by a considerable amount.

Space on the surface of the spacecraft must be available for viewing ports through which laser beams could be transmitted and received from other satellites or the Earth. Additional space on the surface of the spacecraft is required for the radiation cooler which should view essentially dark space for the bulk of the operational time. These space requirements on the surface of the satellite are the only restrictions which cannot be relaxed.

5. CURRENT TECHNOLOGY

Laser technology is expanding rapidly at the present time and it is impossible to write a summary of technology that will be accurate for more than a very short time. The limits of the technology are not in sight and the characteristics of the various devices given below should not in any way be regarded as being representative of the maximum achievable. They are merely what has been attained up to this date, within the limits of the authors' knowledge.

5.1 CARBON DIOXIDE LASERS

Although a great deal of work is currently going on in various aspects of carbon dioxide laser research and development, only those aspects which are directly germane to the proposed program will be discussed.

The Optical Systems Branch awarded a contract in late 1965 to the Electro-Optics Organization of Sylvania Electronics Systems - Western Division, Mountain View, California (NAS5-10309).[9] The purpose of that contract was to develop a carbon dioxide laser capable of producing high power outputs with a high degree of short term frequency stability. The laser produced under this contract utilizes a master-oscillator, power-amplifier to achieve high power simultaneously with high stability and is capable of providing up to 38 watts of single-frequency infra-red radiation in the TEM_{00q} mode. A temperature-controlled oscillator provides 5 watts of power at a single wavelength at 10.6 microns for an active plasma length of 50 cm. The DC-excited amplifier utilizes a folded structure with a total optical path of about 7 meters. A second oscillator, identical to the first, was fabricated to permit heter dyne frequency measurements of the relative stability of the laser. Long-term stability, which was controlled primarily by the thermal environment of the laser, was about ± 3 parts in 10^7. The short-term stability varied between 5 parts in 10^{11} and 1 part in 10^9 over a 10 millisecond time interval. The short-term frequency stability was strongly influenced by the acoustical environment of the laser. The laser oscillator-amplifier combination developed under this program is being used in the laser heterodyne communication system at the Goddard Optical Research Facility, Goddard Space Flight Center. It is shown mounted on a 24" telescope in Figure 5-1. The laser is the long dark box on the left side of the telescope barrel in that photograph.

Since this work for GSFC, Sylvania has been awarded a contract by the NASA Electronics Research Center to produce a space-qualified carbon dioxide laser. This work is currently in progress and should make a large contribution to the work planned for the program described in this proposal.
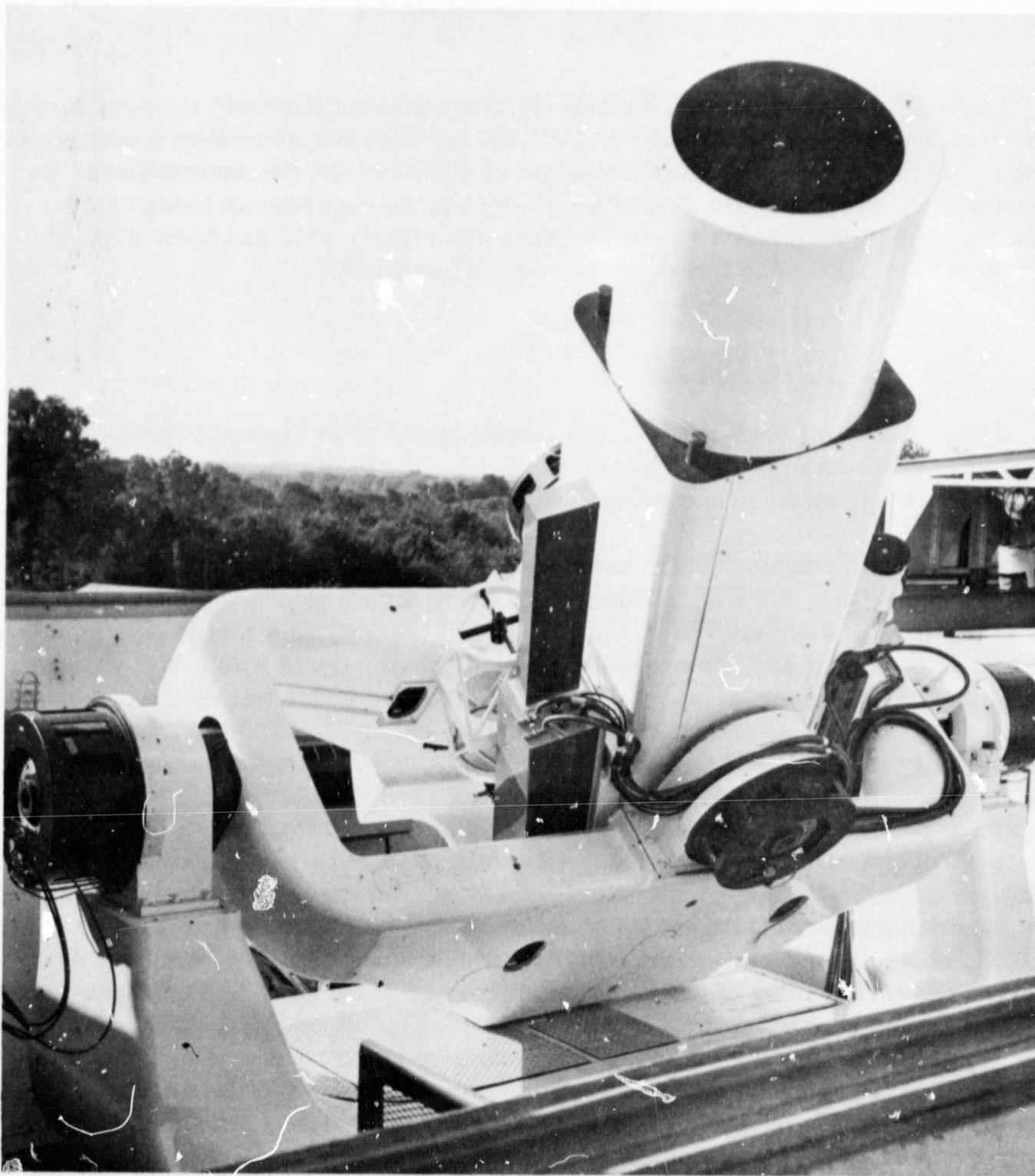
Figure 5-1. 10.6-micron laser heterodyne communication system

The Honeywell, Inc. Systems and Research Division, St. Paul, Minnesota has also been developing small carbon dioxide lasers of a type that would be suitable in a communication system. Under Contract No. NAS8-20645, research and development was performed on "A Frequency Stabilized Carbon Dioxide Laser."[10]

A disassembled view of one of the lasers which has since been produced by Honeywell, Inc. is shown in Figure 5-2. A unique feature of this design is the use of a Cervit block spacer to maintain the mirror spacing at a precise distance and, hence, to assure the frequency stability.

5.2 CARBON DIOXIDE LASER MODULATORS

The Advanced Development Division, GSFC, has sponsored the development of electro-optic modulators for both the 0.9-micron to 3.0-micron region and the 10.6-micron region. A contract entitled, "Development of a 10.6-Micron Modulator" was awarded to the David Sarnoff Research Center of the Radio Corporation of America (NAS5-10144) in early 1966.[11] This contract resulted in the construction of a gallium-arsenide electro-optic modulator employing a 3 mm × 3 mm × 6.7 cm GaAs crystal held between spring loaded parallel plate electrodes. The capacitance of the modulator is 14 picofarads. Two high resistivity Germanium Brewster angle stacks which serve as polarizers and a cadmium sulfide quarter-wave plate complete the unit. A variable-frequency modulating voltage was applied to the modulator and the frequency was varied from dc to 20 MHz. The resulting modulation of a laser beam passing through the crystal was found to be constant over the entire range with the exception of the points where piezoelectric resonances occurred. A photograph of the disassembled modulator is shown in Figure 5-3.

As a part of the Laser Communication Experiment for ATS-F, the Advanced Development Division is continuing to study various types of modulation techniques including internal-cavity techniques and optical-induced free carrier modulation.[12]

5.3 10.6-MICRON DETECTORS

Work carried out under Contract No. NAS5-10156 has resulted in the production by Airborne Instruments Laboratory of a high-sensitivity, field-packaged, 10.6-micron heterodyne mixer and preamplifier. An NEP (noise equivalent power) of 7.5×10^{-20} watt/Hz was measured at an IF of 10 KHz. In the range from 15 MHz to 800 MHz, a receiver NEP of 1.3×10^{-19} watt/Hz was obtained and, in the range up to 1 GHz, an NEP of 2.3×10^{-19} watt/Hz was measured.[13] These sensitivities are only slightly above the quantum noise limit for 10.6-micron radiation, 1.88×10^{-20} watt/Hz. The detector is shown in Figure 5-4.

Only recently, 10.6-micron detectors have become available which can give fast, sensitive response at relatively high operating temperatures, 100°K and even somewhat higher. Among these are the HgCdTe detectors mentioned previously in this document. A task of the proposed program will be to explore the
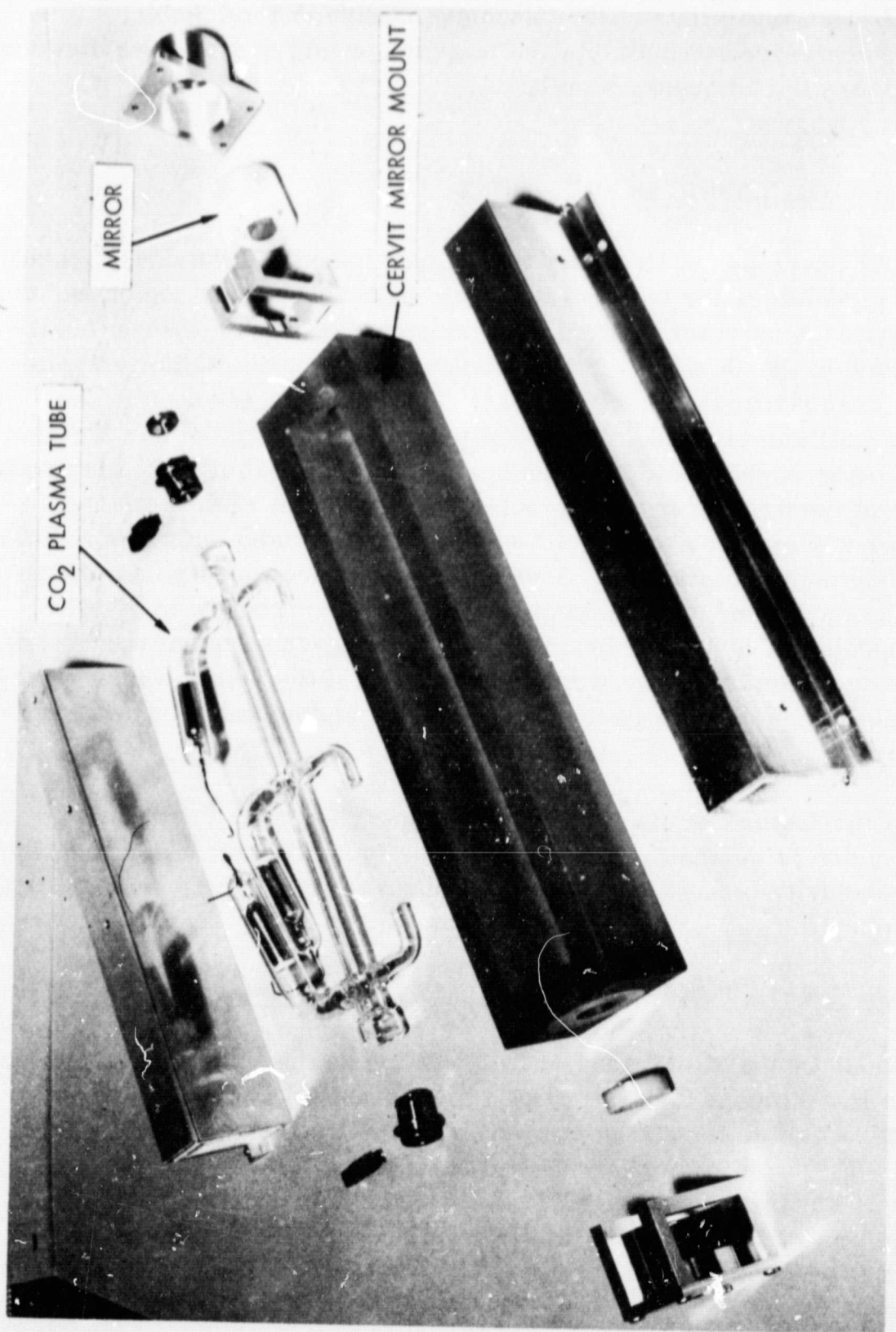
MIRROR

CERVIT MIRROR MOUNT

CO_2 PLASMA TUBE
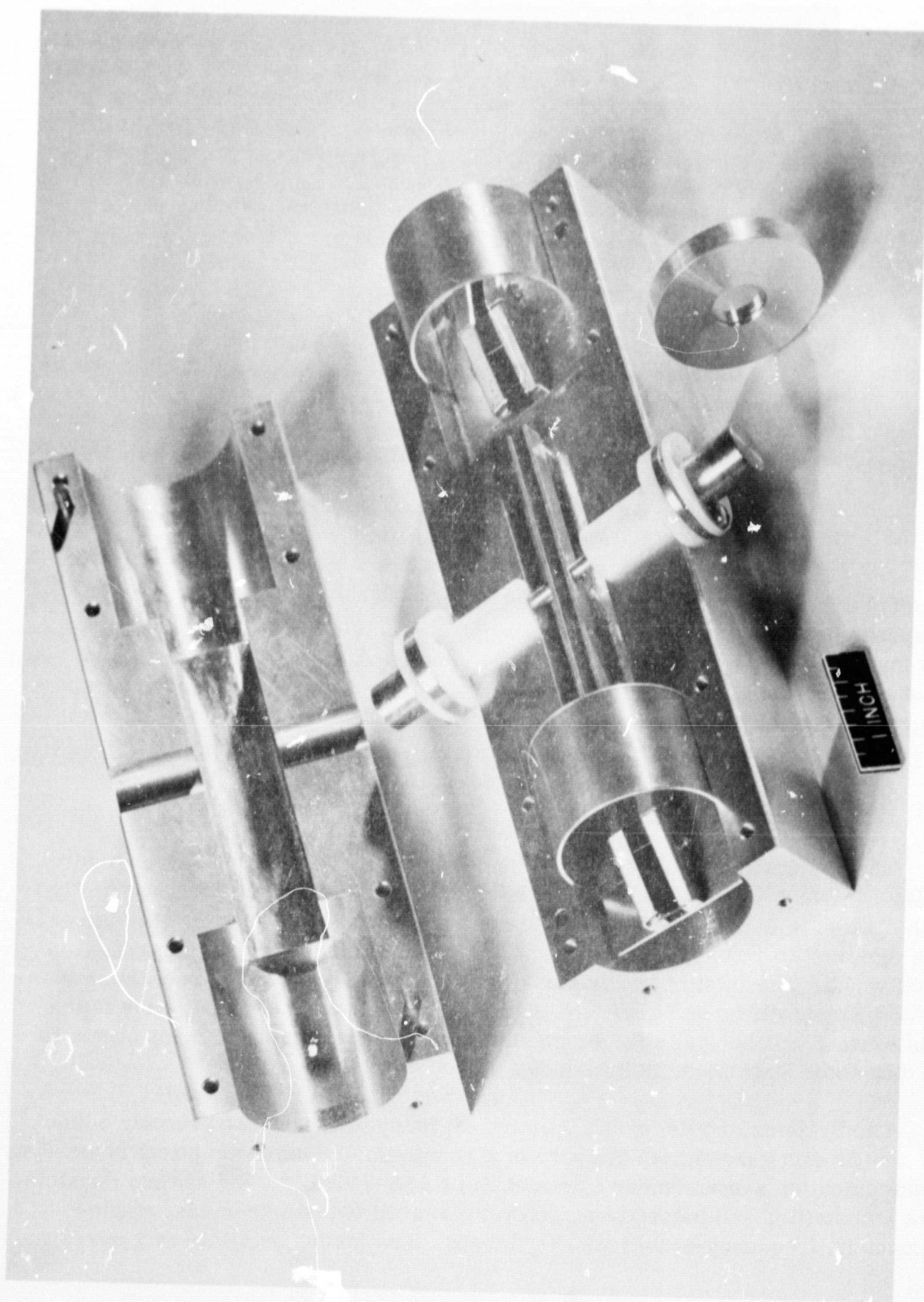
Figure 5-2. Dismantled CO_2 laser

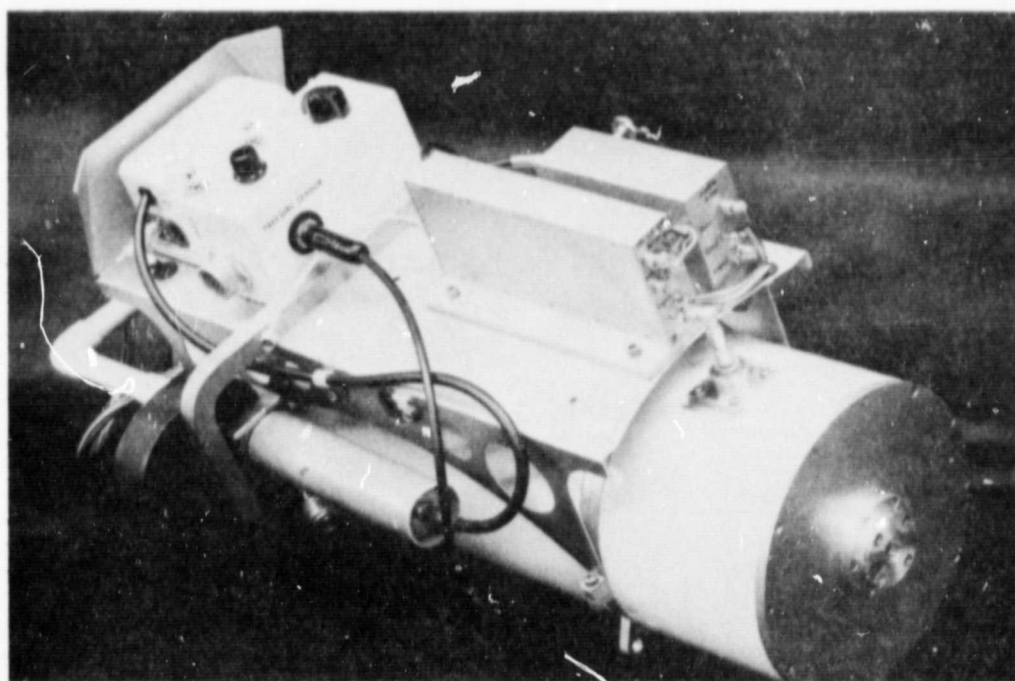Figure 5-3. 10.6-micron GaAs electro-optic modulator

Figure 5-4. Gigahertz bandwidth infrared mixer

precise upper frequency and temperature limitations of these devices. Measured
response has been observed well in excess of 150 MHz, but the upper limit is not
yet known. Other techniques than simple photoconductive detection are also being
studied at present. Preliminary results give some hope that room temperature
operation may be achievable.

5.4 10.6-MICRON SYSTEMS

The system shown in Figure 5-1 and diagrammed in Figure 5-5 is under-
going final test and assembly at the Goddard Optical Research Facility, GSFC.
The system is a complete heterodyne communication system employing the car-
bon dioxide laser described in Section 5.1 and the infrared mixer described in
Section 5.3. The first experiments with this system will be to direct the beam
at various satellites and study the Doppler-shifted return signal. In the future
this system will be available for communication experiments of many types, in-
cluding those envisioned in this proposal.

The Systems and Research Division of Honeywell, Inc. has recently com-
pleted the development and delivery of a complete 10.6-micron optical heterodyne
communication system under Contract No. NAS8-20645.[14] The system consists
of a transmitter and heterodyne receiver. It uses two single-mode, single-
frequency, frequency-stabilized CO_2 lasers. The lasers oscillate at a power

10.6μ TRACKING TRANSMITTER AND SUPERHETERODYNE RECEIVER

TRANSMITTING ANTENNA

TRANSMITTED BEAM

RECEIVED BEAM

MODULATOR

LASER

BEAM STEERER

T.V. ACQUISITION SYSTEM

CRYOGENIC I.R. MIXER
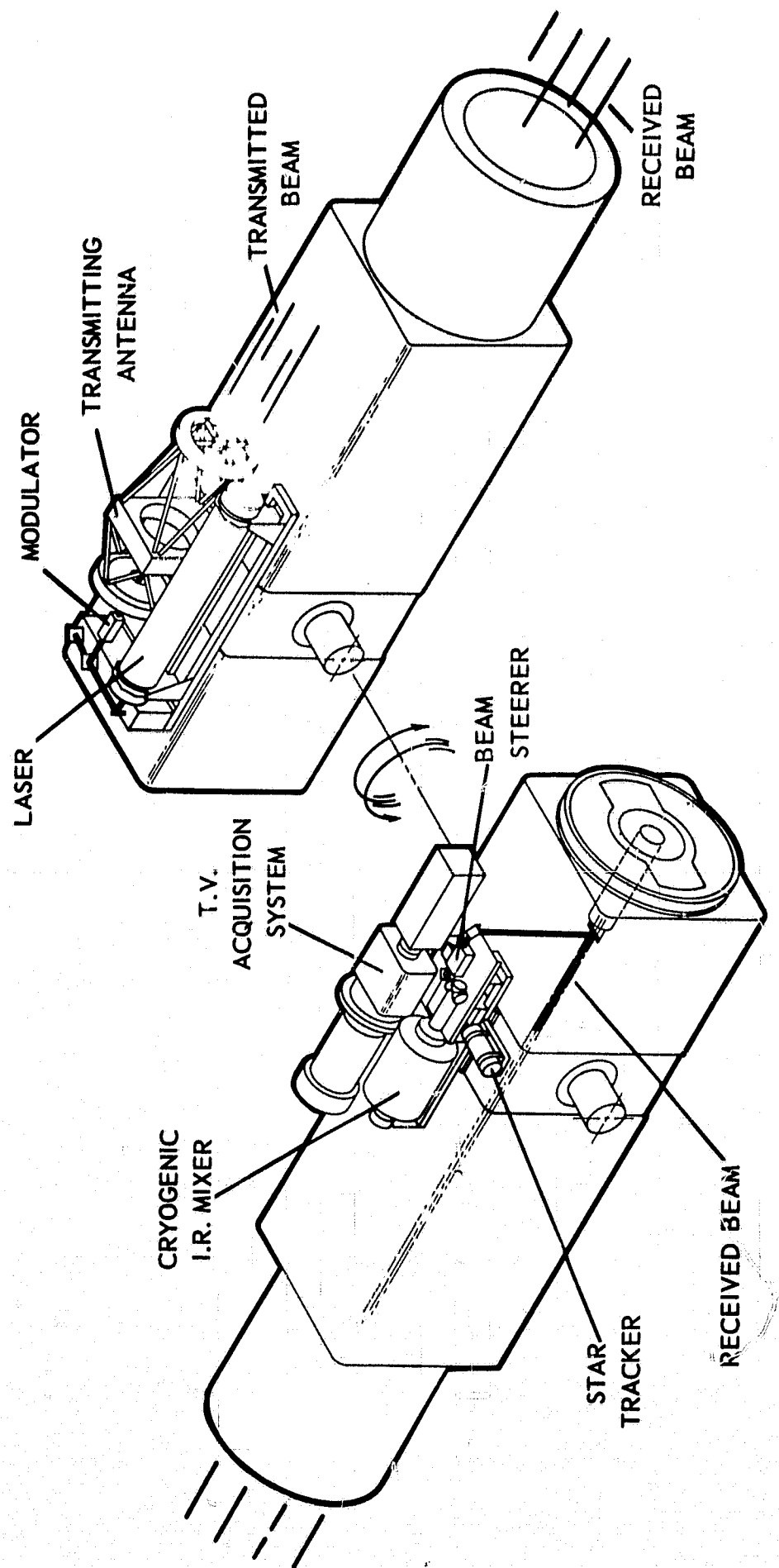
STAR TRACKER

RECEIVED BEAM

Figure 5-5. 10.6-micron laser heterodyne communication system

level of 5 watts with a diffraction-limited beam spread of 5 milliradians. An automatic frequency control loop keeps both lasers locked in frequency with a 10-MHz offset. A frequency stability of 1 part in 10^{10} and a tracking accuracy of 2 parts in 10^{11} have been demonstrated. The system bandwidth is 1 MHz.

Hughes Aircraft Company has assembled a 10.6-micron heterodyne communication system and has broadcast television pictures over a 30-Km path in a wide variety of weather conditions.[15] The success of this link gives a high degree of confidence for the successful completion of the satellite-to-ground experiments proposed in this document. Some of the results obtained in their work are shown in Figure 5-6.

In any optical communication system of the type described in this proposal, a great deal of consideration must be given to the pointing requirements produced by the very high attainable antenna gains. Experience needed to cope with such problems is being gained with systems such as the one shown in Figures 5-1 and 5-5. In addition to this work, the problems of pointing visible laser beams are being successfully addressed. These efforts assure the success of work at the longer, and more easily managed, infrared wavelengths. An example of such a system is the argon laser and ceolostat system shown in Figure 5-7. This system, located at the Goddard Optical Research Facility, has successfully tracked and communicated with a rapidly traveling satellite in a low-altitude orbit, the GEOS-B satellite.

More complex systems have also been developed such as the one shown in Figure 5-8, which was developed by Perkin-Elmer under Contract No. NAS8-20115. This system has the capability of tracking a laser beacon and pointing a transmitted laser beam to within approximately 0.5 microradian. The diameter of the primary optics is approximately 40 cm.[16] The capabilities of this system far exceed the requirements for the proposed program.

Laser communications systems and components, and techniques of optical tracking, have reached the state of development necessary for this proposed experiment, in large part through the optical technology program carried out at NASA centers under direction of Headquarters' Office of Advanced Research and Technology. Pertinent tasks in progress at GSFC under this program are:

- 524-125-22-02-03-51, Stabilized CO_2 Laser

- 524-125-22-02-07-51, Coherent Optical Receiver Studies

- 524-125-22-02-12-51, Optical Instrumentation Development

MEASURED ATTENUATION OF 10.6-MICRON LASER BEAM PROPAGATING OVER A 30 KM HORIZONTAL PATH (HUGHES AIRCRAFT CO. DATA)

WEATHER CONDITION:	CLEAR	HAZE	LIGHT FOG	FOG	LIGHT RAIN
VISIBILITY, Km	100	30	2	1/2	20
TEMPERATURE, °F	66	58	60	58	50
HUMIDITY, %	20	40	40	75	100
ATTENUATION, db/Km ± 0.1	0.54	0.66	0.9	1.9	1.6

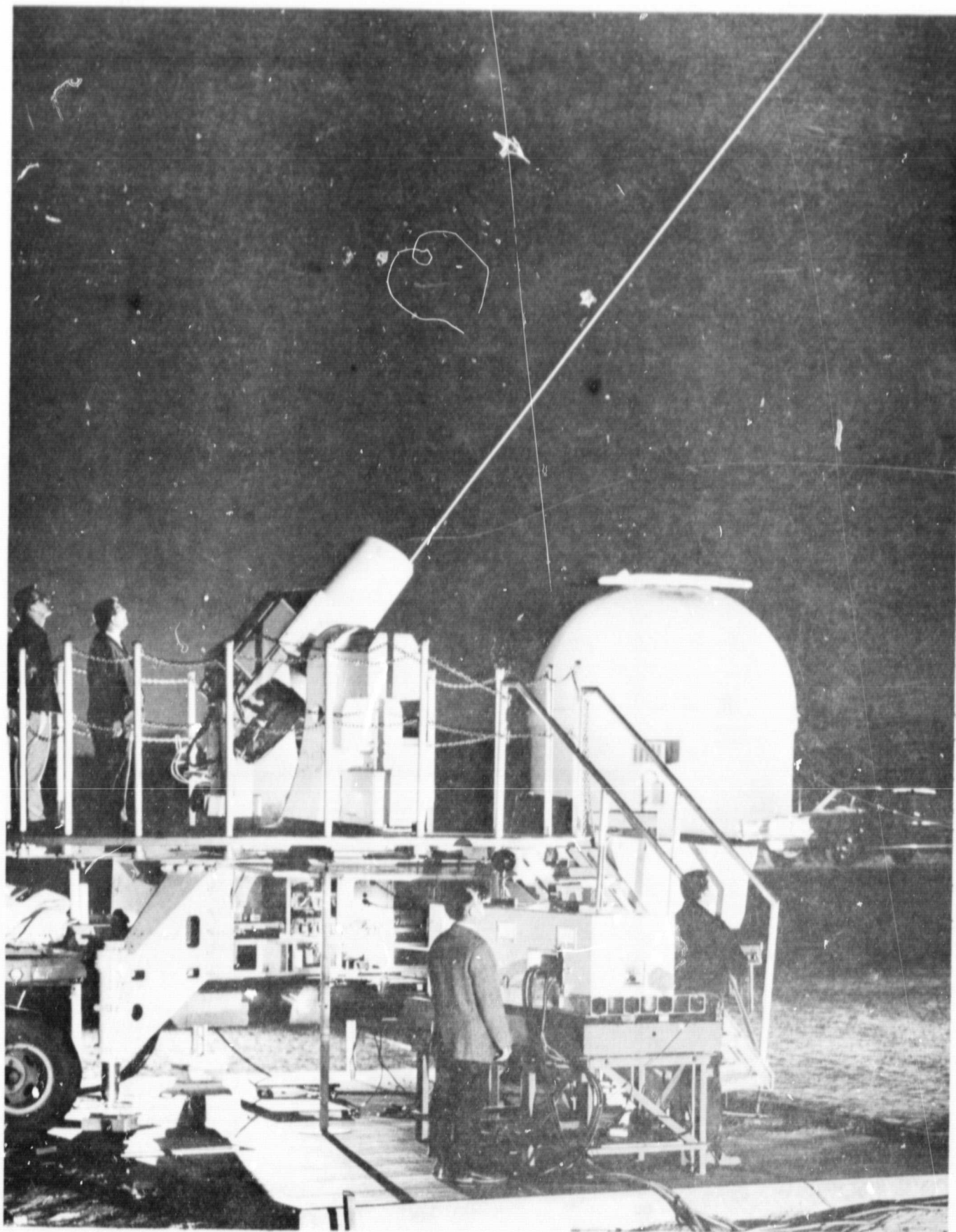Figure 5-6. Performance of a 10.6-micron heterodyne communication system over a 30-Km path

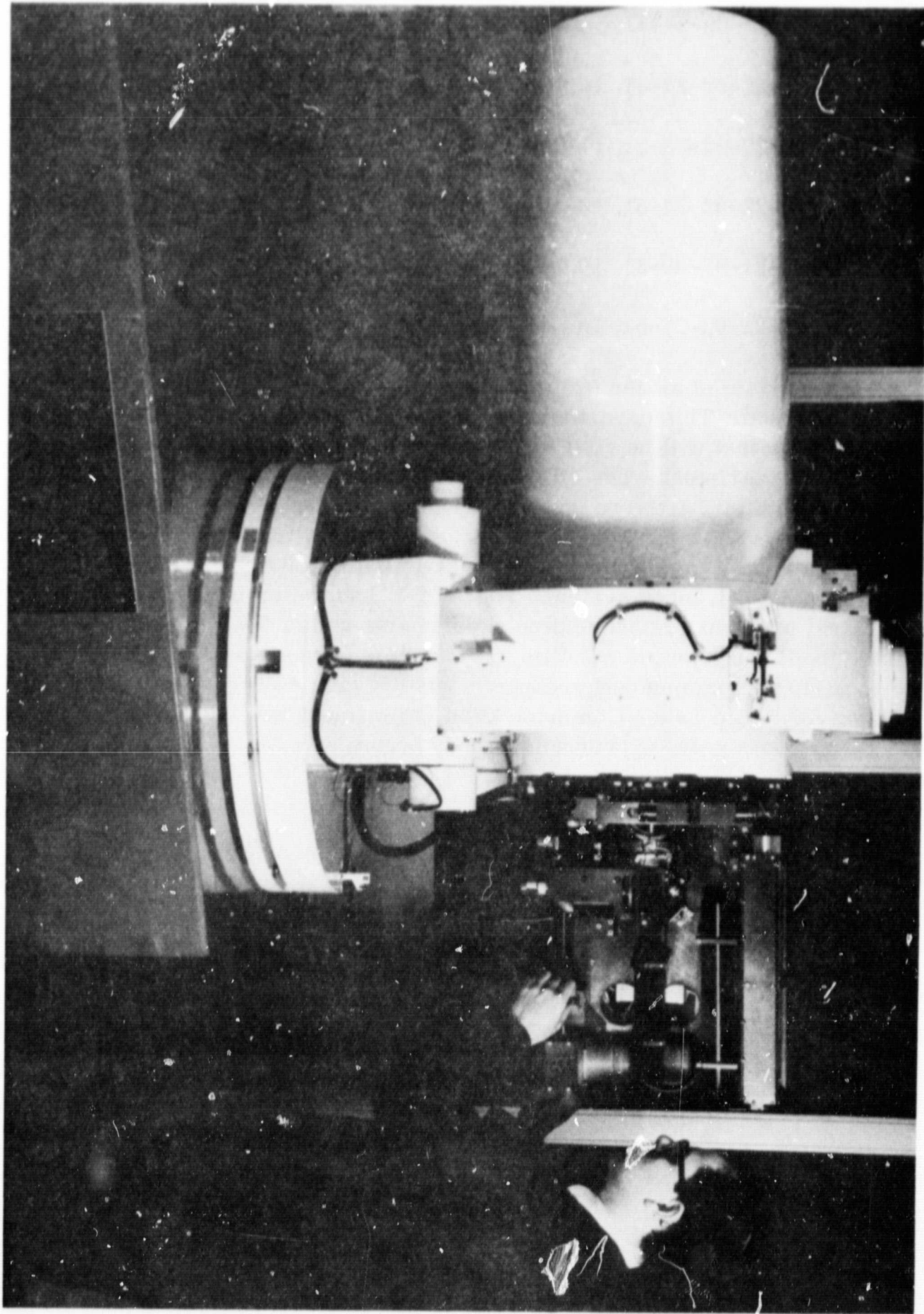Figure 5-7. Precision laser pointing system

Figure 5-8. Precision laser pointing and tracking system

5-11

- 524-125-22-02-24-51, Spacecraft Infrared Retroreflector

- 524-125-22-02-31-51, 10.6-Micron Satellite Experiments

- 524-125-22-02-32-51, Photon-Phonon Interaction Studies

- 524-125-22-02-34-51, 10-Micron Detector Field Package

- 524-125-21-02-09-51, 10.6-Micron D.C. Biased Optical Mixers

- 523-125-21-02-27-51, Laser Modulation

Most appropriate of all the systems discussed is the ATS-F Laser Communication Experiment. This experiment, scheduled to be flown in 1972, is pioneering the technology that will be vital to the success of the proposed advanced laser communication experiment. The ATS-F laser experiment shown in Figure 5-9 will develop the initial hardware that will develop into the advanced system. Optics, detectors, radiation coolers, lasers, modulators, tracking and acquisition systems, and a host of smaller components will be developed and will provide a groundwork for the advanced system. The ATS-F Laser Communication Experiment will first perform communication experiments with a 5-MHz bandwidth between the ATS-F synchronous satellite and a mobile ground station. It is then planned to perform communication experiments between ATS-F and ATS-G. The 10.6-Micron Advanced Laser Communication Experiment will be a logical follow-on and extension of the laser program already begun.
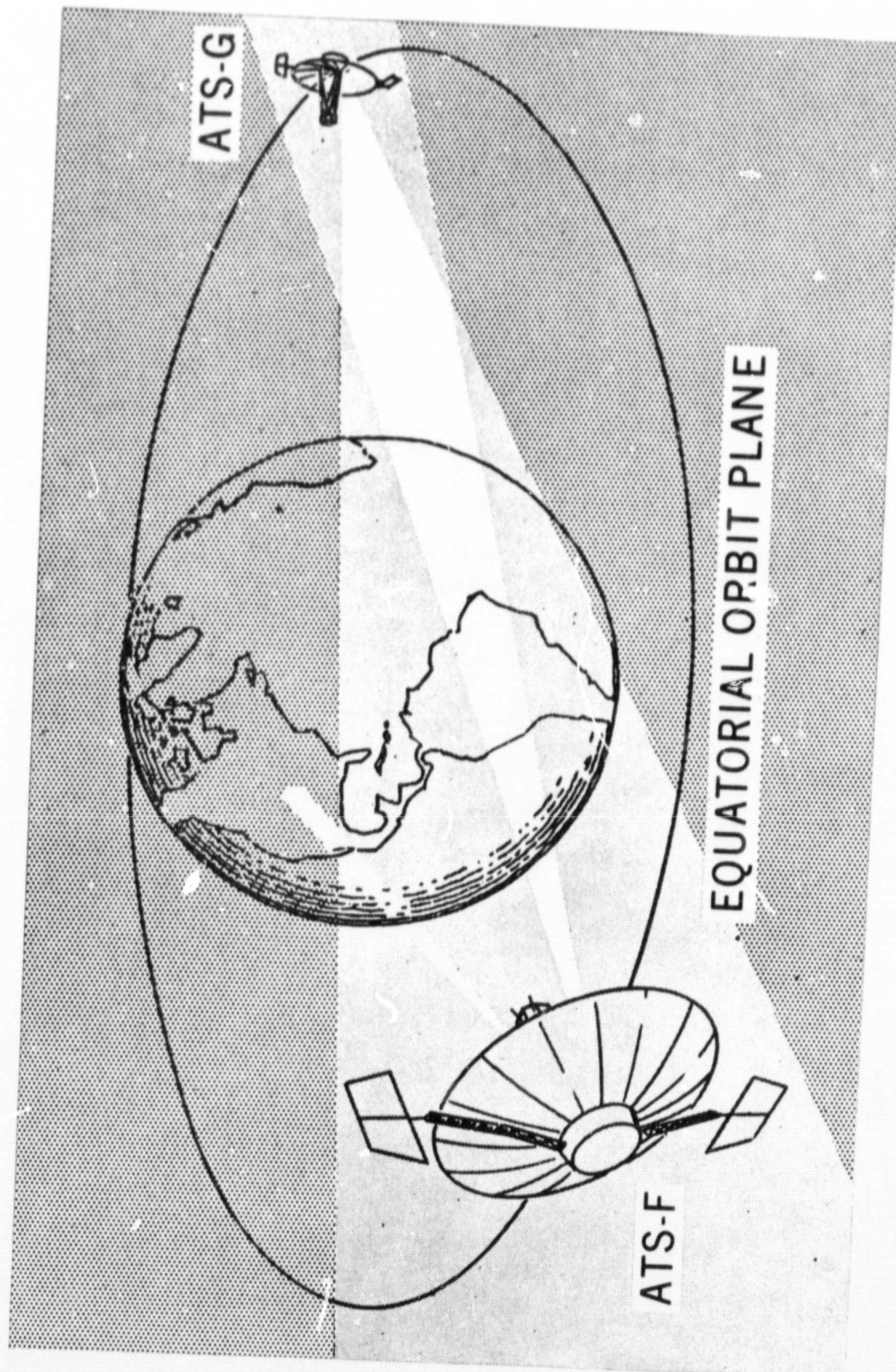
Figure 5-9. ATS-F to ATS-G laser communication link geometry

ATS-G

EQUATORIAL ORBIT PLANE

ATS-F

REFERENCES

1. McAvoy, N., Richard, H. L., McElroy, J. H., and Richards, W. E.: 10.6-Micron Laser Communications System Experiment for ATS-F and ATS-G. NASA TM-X-524-68-206, Goddard Space Flight Center, Greenbelt, Md., May, 1968.

2. Dimeff, J., Gunter, Jr., W. D., and Hruby, R. J.: Spectral Dependence of Deep-Space Communications Capability. IEEE Spectrum, Vol. 4, No. 9, Sept. 1967, pp. 98-104.

3. Wolfe, W. L. (editor): Handbook of Military Infrared Technology. U. S. Government Printing Office, 1965, p. 353.

4. Parker, R. N.: Optical Beam Steering Device. Final Report on Contract No. NAS5-9688, North American Aviation, Inc., Autonetics Division, 18 Jan. 1967.

5. Arams, F., Peyton, B., Sard, E., and Pace, F.: Final Report on High-Sensitivity Infrared Receiver Development. Contract NAS5-10156, July 1967.

6. Teich, M. C., Keyes, R. J., and Kingston, T. H.: Optimum Heterodyne Detection at 10.6 Microns in Photoconductive Ge:Cu. Applied Physics Letters, Vol. 9, No. 10, 15 Nov. 1966, pp. 357-360.

7. Mocker, H. W.: 10.6-Micron Optical Heterodyne Communication System. Phase 3 Report for period 1 August through 31 Oct. 1967 on Contract NAS8-20645, 31 Oct. 1967.

8. Hocker, L. O., Sokoloff, D. R., Daneu, V., Szoke, A., and Jaran, A.: Frequency Mixing in the Infrared and Far-Infrared Using a Metal-to-Metal Point Contact Diode. Applied Physics Letters, Vol. 12, No. 12, 15 June 1968, pp. 401-402.

9. Reynolds, R. S.: Final Report on Stabilized CO_2 Gas Laser (1 Dec. 1966 - 30 Jan. 1968). Contract No. NAS5-10309.

10. Mocker, H. and Gustafson, H.: A Frequency Stabilized Carbon Dioxide Laser. Final Report for period June 22 through Dec. 22, 1966, Contract No. NAS8-20645.

11. Walsh, T.: Development of a 10.6-Micron Laser Modulator. Final Report for period Feb. 18 to July 18, 1966. Contract NAS5-10144.

12. Gruber, C. and Richards, W. E.: Optically Induced Free-Carrier Light Modulator. NASA TN D-4608, June 1968.

13. Arams, F., Peyton, B., Pace, F., Lange, R., and DiNardo, A.: Second Quarterly Report for Phase II of High-Sensitivity Infrared Receiver Development, April 1968, Contract No. NAS5-10156.

14. Mocker, H. W.: A 10.6-Micron Optical Heterodyne Communication System. Sept. 1968, Final Report on Contract No. NAS8-20645.

15. Goodwin, F. E., and Nussmeier, T. A.: Optical Heterodyne Experiments at 10.6 Microns. Paper 10J-5 presented at the 1968 International Quantum Electronics Conference, Miami, Fla., May 14-17, 1968.

16. Lipsett, M. S.: Laser/Optics Techniques Summary Report on Contract NAS8-20115, 29 April 1966.

APPENDIX A

DERIVATION OF WAVELENGTH DEPENDENCE
OF REQUIRED TRANSMITTED POWER
FOR INTERSATELLITE COMMUNICATIONS

The following derivation will show the dependence of the required transmitted power per cycle of bandwidth for intersatellite communications.

Dimeff describes a model for future spaceborne antennas by

$$r^2 = 10^{6.37} f^{-0.48}, \qquad (A-1)$$

where r is the radius of the antenna and f is the frequency of the radiation transmitted or received. While this equation applies to transmitting antennas it is used here for the common receiving and transmitting antennas discussed in this proposal. In terms of d, the antenna diameter, and λ, the radiation wavelength, Equation (A-1) becomes

$$d^2 = 8.06 \times 10^2 \lambda^{0.48}. \qquad (A-2)$$

Antenna gain, G, can be defined by

$$G = 4\pi/\Omega, \qquad (A-3)$$

where Ω (for small angles) is nearly the square of the beamwidth between the two half-power points on the radiation pattern, i.e. $(\lambda/d)^2$. Therefore,

$$G = 4\pi d^2/\lambda^2. \qquad (A-4)$$

Substituting d^2 from Equation (A-2) yields

$$G = 4\pi \times 8.06 \times 10^2 \lambda^{-1.52}. \qquad (A-5)$$

The power collected by a receiving antenna is given by the range equation:

$$P_R = \frac{P_T G_T G_R \lambda^2}{(4\pi R)^2}, \tag{A-6}$$

where P_R and G_R, P_T and G_T represent the received power and receiver antenna gain and transmitted power and transmitter antenna gain, respectively, and R is the range between transmitting and receiving systems.

Introducing T_R to represent the fractional transmission of the optical system between the receiver antenna and the signal detector gives

$$P_S = T_R P_R = \frac{T_R P_T G_T G_R \lambda^2}{(4\pi R)^2}. \tag{A-7}$$

By setting G_T equal to G_R and by making use of (A-5), we have

$$P_S = 6.5 \times 10^5 T_R P_T \lambda^{-1.04}/R^2. \tag{A-8}$$

An expression for the noise power, P_N, is given by[*]

$$P_N = \left[\frac{hf}{e^{hf/kT} - 1} + hf\right] B, \tag{A-9}$$

where h is Planck's constant, B is the system noise bandwidth, k is Boltzmann's constant, f is the laser carrier frequency, and T is the noise equivalent temperature of the receiver in degrees Kelvin. The signal-to-noise power ratio can then be written as

$$(S/N)_P = \frac{6.5 \times 10^5 T_R P_T \lambda^{-1.04}/R^2}{\left[\dfrac{hf}{e^{hf/kT} - 1} + hf\right] B}. \tag{A-10}$$

---

[*]Oliver, B. M.: Thermal and Quantum Noise. Proc. of the IEEE, Vol. 53, No. 5, May 1965, pp. 436-454.

Solving for P_T gives

$$P_T = \frac{(S/N)_P\, R^2\, \lambda^{1.04}}{6.5 \times 10^5\, T_R}, \qquad\qquad (A\text{-}11)$$

or

$$P_T = K\, P_N(\lambda)\, \lambda^{1.04}, \qquad\qquad (A\text{-}12)$$

where K, a defined normalizing constant, removes all but wavelength dependent terms.

APPENDIX B

DERIVATION OF DOPPLER FREQUENCY SHIFT
ON LINK BETWEEN SYNCHRONOUS AND
LOW-ALTITUDE SATELLITE

The standard expression for the Doppler shifts resulting from a relative velocity between transmitter and receiver is

$$f' = f_o \left[\frac{1 - \dfrac{dR/dt}{c}}{1 + \dfrac{dR/dt}{c}} \right] . \tag{B-1}$$

In this expression f' represents the shifted frequency, f_o the original frequency, dR/dt the relative velocity between transmitter and receiver, and c is the speed of light. This equation leads to the approximation

$$f' \cong f_o \left(1 - \frac{2dR/dt}{c} \right) . \tag{B-2}$$

Solving for dR/dt gives

$$dR/dt \cong c\Delta f / 2 f_o , \tag{B-3}$$

where $\Delta f = f_o - f'$.

Knowing dR/dt, or v_{rel} and v_T, the low-altitude satellite's tangential velocity determines ψ (see Figure 2-15). Since $\alpha = 90° + \psi$,

$$\frac{L}{\sin \alpha} = \frac{L}{\sin (90° + \psi)} = \frac{r_N}{\sin \beta} , \tag{B-4}$$

where L is the distance between the synchronous satellite and the center of the Earth and r_N is the distance between the center of the Earth and, for example, Nimbus. Solving for β gives

$$\beta = \sin^{-1}\left[\frac{r_N \sin(90° + \psi)}{L}\right].\qquad\text{(B-5)}$$

By construction,

$$\Omega = 180° - (\beta + \alpha),\qquad\text{(B-6)}$$

or, upon substitution,

$$\Omega = 180° - \left\{\sin^{-1}\left\{\frac{r_N \sin\left[90° + \cos^{-1}\left(\frac{v_{rel}}{v_T}\right)\right]}{L}\right\} + \left[90° + \cos^{-1}\left(\frac{v_{rel}}{v_T}\right)\right]\right\}.$$

$$\text{(B-7)}$$

And, upon further substitution,

$$\Omega = 180° - \left\{\sin^{-1}\left\{\frac{r_N \sin\left[90° + \cos^{-1}\left(\frac{\Delta f\, c}{2 f_o v_T}\right)\right]}{L}\right\} + \left[90° + \cos^{-1}\left(\frac{\Delta f\, c}{2 f_o v_T}\right)\right]\right\}$$

$$\text{(B-8)}$$

A plot of Δf as a function of Ω appears in Figure 2-17.